Alberto F. Maroto[1,2,3], Mireia Borrajo[1,2,3], Àngela Callejo[4,5], Emilio Amilibia[4,5], Marta Pérez-Grau[4,5], Francesc Roca-Ribas[4,5], Elisabeth Castellanos[5,6], Alejandro Barrallo-Gimeno[1,2,3], Jordi Llorens[1,2,3]

The vestibular calyceal junction is dismantled in response to diverse injuring stimuli in rats and humans

[1] Departament de Ciències Fisiològiques, Universitat de Barcelona (UB), Feixa Llarga s/n, 08907 l'Hospitalet de Llobregat, Catalunya, Spain.

[2] Institut de Neurociències, Universitat de Barcelona (UB), Barcelona, Catalunya, Spain.

[3] Institut d'Investigació Biomèdica de Bellvitge (IDIBELL), 08907 l'Hospitalet de Llobregat, Catalunya, Spain.

[4] Servei d'Otorinolaringologia, Hospital Universitari Germans Trias i Pujol, Badalona, Catalunya, Spain.

[5] CSUR Phakomatoses Multidisciplinary Clinics HUGTIP-ICO-IGTP, Barcelona, Catalunya, Spain.

[6] Clinical Genomics Research Group, Institut de Recerca Germans Trias i Pujol (IGTP), Badalona, Catalunya, Spain.

Corresponding author: Prof. Jordi Llorens, Ph.D.; e-mail: jllorens@ub.edu; Ph: +34934024277

E-mail addresses and ORCID codes:

A.F.M.: albertomaroto@hotmail.com; 0000-0001-8265-4902

M.B.: mborrajoarjona@ub.edu; 0000-0003-2126-5713

A.C.: angelacallejo@gmail.com; 0000-0003-3820-7405

E.A.: emilioamilibia@gmail.com; 0000-0003-0587-7891

M.P.G.: martaperezgrau@gmail.com; 0000-0003-4630-0116

F. R.R.: francescrocaribas@gmail.com; 0000-0001-6620-8216

E.C.: ecastellanos@igtp.cat; 0000-0002-8133-5325

A.B.G.: abarrallo@ub.edu; 0000-0003-2086-8926

J.L.: jllorens@ub.edu; 0000-0002-3894-9401

Acknowledgements

This study was supported by grant number RTI2018-096452-B-I00 (Ministerio de Ciencia e Innovación, Agencia Estatal de Investigación, MCIU/AEI, 10.13039/501100011033, and European Regional Development Fund, FEDER), grant number 2017SGR621 (Agència de Gestió d'Ajuts Universitaris i de Recerca, AGAUR, Generalitat de Catalunya), and grant number 202007-30-31 (Fundació La Marató de TV3 2019) . A.B.G is a Serra-Húnter fellow. The electron and confocal microscopy studies were performed at the Centres Científics i Tecnològics de la UB (CCiTUB) of the Universitat de Barcelona. We thank Benjamín Torrejon-Escribano, Rosa Rivera, Adriana Martínez Gené, Josep Manel Rebled and Eva Prats for the expert and technical help. We also thank Dr Bechara Kachar for the generous gift of the KCNQ4 antibody.

Competing interests

The authors declare no competing interests

ABSTRACT

Hair cell (HC) loss by epithelial extrusion has been described to occur in the vestibular system of rats and mice during the chronic ototoxicity caused by 3,3'-iminodipropionitrile (IDPN). This is preceded by early dismantlement of the calyceal junction in the contact between type I HC (HCI) and calyx afferent terminals. In the present study, we evaluated whether these pathological phenomena have wider significance. First, we assessed their occurrence in rats receiving streptomycin for 3 to 8 weeks. Streptomycin caused a loss of vestibular function that was largely reversible and associated with a partial loss of HCI. In the calyces encasing the surviving HCI, we observed decreased expression of CASPR1 denoting calyceal junction dismantlement. We also recorded reduced numbers of pre-synaptic (ribeye) and post-synaptic (PSD95) puncta per cell, and KCNQ4 mislocalization. After washout, the CASPR1 label revealed calyceal junction rebuilding. Ultrastructural data also showed calyx junction dismantlement and calyx fragmentation. Limited but clear evidence for HC extrusion was obtained by scanning electron microscopy and immunofluorescent analysis. Second, we evaluated human sensory epithelia from therapeutic labyrinthectomy and trans-labyrinthine. In some of the samples, patched CASPR1 label indicated that a process of calyx junction dismantlement could be in progress. The present data supports the hypothesis that dismantlement of the calyceal junction is a common response triggered by chronic stress in the vestibular sensory epithelium. This effect precedes HC loss, is reversible, and may explain, at least in part, observations of reversion in function loss.

55 **INTRODUCTION**

56 Sensory encoding by the inner ear's vestibular system depends on the transducing function of hair cells (HC). In
57 most mammals, these cells do not regenerate to a significant extent, so permanent loss of equilibrium and gaze
58 control occurs as a result of HC loss. Nevertheless, significant recovery in vestibular function is recorded clinically
59 in a variety of disease conditions. In some cases, such as benign paroxysmal positional vertigo (von Brevern et
60 al., 2015), recovery is complete, suggesting that the condition is associated with pathogenic mechanisms that
61 transiently impair the system's function but do not cause HC loss. In other disease condition, such as Ménière's
62 disease (López-Escámez et al., 2015), recurrent crisis often associate with incomplete recovery and progressive
63 worsening of the vestibular function. In the case of exposure to ototoxic aminoglycoside antibiotics, irreversible
64 loss of vestibular function is a common outcome (Black et al., 2004) but significant yet incomplete recovery has
65 also been recorded (Black et al., 2001). In recent years, we have used a sub-chronic ototoxicity model to identify
66 reversible cellular and molecular alterations in the vestibular epithelia that associate with reversible loss of
67 vestibular function in rats (Sedó-Cabezón et al., 2015) and mice (Greguske et al., 2019). These studies showed
68 that the sub-chronic ototoxic stress caused by the experimental compound 3,3'-iminodipropionitrile (IDPN)
69 results in dismantlement of the calyceal junction between type I HCs (HCI) and the calyx afferent terminals, as
70 demonstrated by ultrastructural criteria and by loss of the junction proteins CASPR1 (contactin-associated
71 protein) and tenascin-C, as well as delocalization of the voltage-gated potassium channel KCNQ4.
72 Simultaneously, the vestibular epithelium showed loss of pre-synaptic and post-synaptic puncta indicative of
73 synaptic uncoupling between the HCs and their afferents. These changes associated with loss of vestibular
74 function as revealed by behavioural deficits. In this model, if the exposure was halted at an early stage of the
75 toxicity, both the epithelium alterations and the behavioural dysfunction were largely reversible. In contrast, if
76 the exposure was maintained, the function loss became persistent as a result of HC loss that predominantly
77 occurred by extrusion of live cells from the sensory epithelium to the endolymphatic cavity (Llorens and
78 Rodríguez-Farré, 1997; Seoane et al., 2001a,b; Sedó-Cabezón et al., 2015; Greguske et al., 2019).

79 The rat and mouse sub-chronic IDPN models illustrate a cellular pathway to HC demise that differs from
80 apoptosis (Seoane et al., 2001a). As explained in the previous paragraph, it is ended by extrusion after a phase of
81 sensory cell detachment and synaptic uncoupling (Sedó-Cabezón et al., 2015; Greguske et al., 2019). The fact
82 that extrusion is the main form of HC demise in birds and amphibians following a variety of insults (Hirose et al.,
83 1999; Rubel et al., 2013) suggests that its molecular mechanisms may be highly conserved across vertebrates
84 and operate in response to damage of diverse origin. Surprisingly, this phenomenon has received scarce
85 attention and information is lacking about its molecular mechanisms and relevance to human health. One first
86 question worth to address is whether these phenomena have a role in mammalian aminoglycoside toxicity *in*
87 *vivo*, as this is the main cause of vestibular toxicity in humans. Although most research on aminoglycoside-
88 induced HC loss has focused on apoptosis (Furness, 2015), the literature also contains evidence that these drugs
89 may cause vestibular HC extrusion (Li et al., 1995; Nakagawa et al., 1997; Granados and Meza, 2005). In the
90 present work, we studied whether dismantlement of the calyceal junction, synaptic uncoupling and HC extrusion
91 occur in the rat vestibular epithelium in response to one aminoglycoside antibiotic, streptomycin. Previously, we
92 found that the mode of HC demise, extrusion, apoptosis or necrosis was determined by the intensity and
93 duration of the toxic stress. Thus, high acute doses of IDPN caused HC necrosis, sub-acute exposure to medium
94 doses caused HC apoptosis and sub-chronic low dose exposure elicited HC extrusion (Seoane et al., 2001a).
95 These data indicate that short exposure paradigms aimed at accelerating and synchronizing HC demise (Taylor et
96 al., 2008; Oesterle et al., 2008; Benkafadar et al., 2021) may in fact favour the apoptotic pathways in front to
97 other possible pathways. Accordingly, in the present study we studied the effects of sub-chronic aminoglycoside
98 exposure. As a second approach to evaluate the relevance of these phenomena to human disease conditions,
99 we explored their occurrence in vestibular epithelia from a substantial number of patients of vestibular
100 schwannoma and a few from other vestibular diseases requiring also trans-labyrinthine tumour excision
101 (meningioma and endolymphatic sac tumour) or therapeutic labyrinthectomy (Ménière's disease). Vestibular
102 schwannomas are tumours that grow in the vestibular nerve and cause hearing and vestibular function loss.

103 Current evidence indicates that this loss may in part be caused by the negative impact on the sensory epithelia

104 of pro-inflammatory factors secreted by the tumour (Dilwali et al., 2015). The data we obtained demonstrate

105 that calyceal junction dismantlement occurs during chronic streptomycin toxicity in rats and provide evidence

106 that it occurs in human vestibular epithelia in response to other kinds of stress.

107 **RESULTS**

108 **Effects of streptomycin sulphate on body weight and overall health.**

109 To study the sub-chronic toxicity of streptomycin on the vestibular system, we administered male and female
110 rats with one daily dose of streptomycin sulphate (0, 100, 300, 400 or 500 mg/kg x day - groups CTRL, STR-100,
111 STR-300, STR-400, STR-500) for up to 6 or 8 weeks, starting at day 21 of age. Other groups of rats were
112 administered with two daily doses of 0, 300, 350 or 400 mg/kg - groups CTRL, STR-300x2, STR-350x2, STR-
113 400x2). Rats administered with streptomycin showed an acute sedative effect starting within few minutes after
114 each daily dose, most evident in the high dose (STR-500) group: the animal stayed quiet, with decreased
115 responsiveness and with an overtly low muscle tone. This effect usually lasted 15-20 min but sometimes lasted
116 for up to two hours after injection. During this sedation period, two rats died in the STR-500 group at days 5 and
117 36, likely from respiratory arrest. Also, two rats died for unknown reasons after 20 and 37 days in the STR-300
118 and STR-500 groups, respectively. No animals died when larger daily doses were administered divided in two
119 daily injections. Recovery from this sedative effect was complete and surviving animals showed normal
120 behaviour except for the evidences of vestibular dysfunction explained below. As shown in Supplementary
121 Figure S1, streptomycin animals showed an increase in body weight smaller than that shown by control rats. This
122 resulted in significant differences from control body weights in the streptomycin animals after five or more
123 weeks of one daily dose, and by two weeks in the streptomycin groups receiving two daily doses.

124 **Loss and recovery of vestibular function after sub-chronic streptomycin exposure.**

125 Sub-chronic exposure to streptomycin sulphate caused a dose-dependent loss of vestibular function as indicated
126 by the rat's abnormalities in spontaneous motor behaviour. Vestibular deficient animals showed ataxia,
127 spontaneous circling and head bobbing. The loss of function was assessed using high-speed video records of the
128 tail-lift reflex as described (Martins-Lopes et al., 2019; Maroto et al., 2021a,c). A similar dose-dependent effect
129 occurred in male and female animals, and therefore animals of both sexes were pooled for analyses. The

130 decrease in tail-lift angles, indicative of loss of vestibular function, was not significant in the STR-100 group, and
131 smaller in the STR-300 and STR-400 groups compared to the STR-500 group (Suppl. Fig. S2), so further analysis
132 on the one daily dose paradigm focused on this dose level. As shown in Figure 1A, a progressive reduction in tail-
133 lift angles was recorded in the STR-500 rats. Repeated-measures MANOVA of the tail-lift data from days 0 (pre-
134 test) to 42 resulted in significant day ($F[6,28]=15.38$, $p<0.001$), treatment ($F[1,33]=18.0$, $p<0.001$), and day X
135 treatment interaction ($F[6,28]=9.766$, $p<0.001$) effects, with significant differences between CTRL and STR-500
136 mean values recorded at 4 to 6 weeks of exposure. Extension of the administration up to 8 weeks caused only a
137 modest additional effect on vestibular function (Suppl. Fig. S3A).

138 By administering streptomycin in two daily injections, larger doses could be given to the animals and circumvent
139 the risk of death associated with the acute sedative effects of the drug. As shown in Fig. 1B, all the STR-300x2,
140 STR-350x2, and STR-400x2 groups showed faster and deeper loss of vestibular function than the STR-500 group.
141 MANOVA of the tail-lift data from the two injections experiment up to day 21 resulted in significant day
142 ($F[3,26]=191.1$, $p<0.001$), treatment ($F[3,28]=45.89$, $p<0.001$), and day X treatment interaction ($F[9,63.4]=20.92$,
143 $p<0.001$) effects. The effect was dose-dependent, and larger doses caused a faster progression of the decline in
144 vestibular function.

145 To evaluate the potential for functional recovery, some animals were allowed to survive after the end of the
146 sub-chronic streptomycin exposure. As shown in Fig. 1C, rats exposed to 500 mg/kg · day of streptomycin for 6
147 weeks recovered normal tail-lift angles during the washout period. Functional recovery was also observed in the
148 STR-500 rats exposed for 8 weeks (Suppl. Fig. S3B). The individual values of animals allowed to recover after 3
149 weeks of two daily doses of streptomycin also showed a clear recuperation of the tail-lift reflex (Fig. 1D).

150 **Sub-chronic streptomycin exposure caused partial loss of HCs in the vestibular sensory epithelia.**

151 To evaluate the major effects of streptomycin on the vestibule, we observed surface preparations of the sensory
152 epithelia using scanning electron microscopy (SEM). As reported in previous studies (Llorens et al., 1993; Seoane

153 et al., 2001a; Sedó-Cabezón et al., 2015), SEM observation of control epithelia (n=16) (Fig. 2A; Suppl. Fig. S4A, B)
154 revealed morphological features matching literature descriptions of healthy untreated rats, with high densities
155 of stereocilia bundles. Epithelia from STR-300 animals (6 weeks of exposure, n=3) showed similar features to
156 control epithelia, except for the signs of a few missing hair bundles or occasional bundles with fused stereocilia
157 (data not shown). In animals administered once a day with larger doses of streptomycin, the SEM observations
158 revealed from scant to moderate loss of stereocilia bundles. Similar findings were obtained in STR-500 rats, with
159 small difference between animals exposed for 6 (n=6) or 8 (n=7) weeks, and in STR-400 rats exposed for 8 weeks
160 (n=2). The hair bundle loss was roughly similar in cristae (Suppl. Fig. S4C), utricles (Suppl. Fig. S4D) and saccules
161 (Fig 2B, C), with no evidence for an overt difference in susceptibility among receptors. In all cases, the loss of
162 stereociliary bundles was partial and many bundles were still present in the sensory receptors of the worst cases
163 (Suppl. Fig. S4E,F). In these SEM observations, images indicating ongoing damage were scarce. Nevertheless,
164 some evidence for fused stereocilia and HC protrusion were found (Fig 2D,E). Animals given two daily injections
165 of streptomycin displayed a larger loss of stereociliary bundles than the animals administered once a day (Suppl.
166 Fig. S5). Evidence for ongoing damage was scarce in some epithelia, but clear in other samples. These included
167 images of epithelial scars, bundle fusion and cell protrusion towards the endolymphatic cavity (Suppl. Fig. S5).
168 The average extent of hair bundle loss was similar in STR-300x2 rats treated for 6 weeks (n=7), STR-350x2 rats
169 treated for 4 weeks (n=6), and STR-400x2 rats treated for 3 weeks (n=6).

170 To determine the loss of HCs revealed by the decreased densities of hair bundles observed by SEM in STR-500
171 rats, we obtained type I HC (HCI) and type II (HCII) counts from the vestibular epithelia of the other ear of the
172 same animals. To this end, we immunostained the epithelia with antibodies against myosin-7a (MYO7A),
173 CASPR1, and the calcium-binding protein calretinin, revealed by fluorescent secondary antibodies. In the
174 confocal microscopy images, HCI were identified as MYO7A+ cells (a pan-HC marker, Hasson et al., 1997)
175 surrounded by a CASPR1+ calyx (Sousa et al., 2009; Lysakowski et al., 2011; Sedó-Cabezón et al., 2015), even if
176 weak or fragmented, or with an unambiguous HCI shape, with a long and narrow neck. As an estimate of HCII,

177 we counted cells with double MYO7A and calretinin label (Dechesne et al., 1991). The data obtained, presented
178 in Fig. 3, reveal a significant decrease in HCI counts in both peripheral and central/striola regions of the crista
179 and the utricle and in the peripheral saccule. ANOVA results were: central crista, $F[3,27]= 12.82$, $p<0.001$;
180 peripheral crista, $F[3,24]=2.89$, $p=0.056$; central utricle $F[3,25]=23.86$, $p<0.001$; peripheral utricle, $F[3,26]=44.95$,
181 $p<0.001$; central saccule, $F[3,20]=2.01$, $p=0.15$ - N.S.; peripheral saccule, $F[3,22]=8.31$, $p=0.001$. The most
182 affected receptor was the utricle, with a 52-67 % decrease in HCI counts in STR-500 animals, followed by the
183 crista, where a 30-40 % loss was recorded. In both the crista and the utricle, similar effects were recorded in
184 animals exposed for 6 weeks and animals exposed for 8 weeks. In the saccule, the loss was smaller than in crista
185 and utricle receptors, and apparently greater at 8 than at 6 weeks of treatment. HCI counts remained reduced in
186 animals allowed to recover after the end of the exposure period. In contrast to HCI, no significant differences
187 were obtained among treatment groups in HCII counts (all p values > 0.1).

188 As explained above, the SEM observations indicated a loss of HC after two daily injections of streptomycin
189 greater than that recorded after one daily injection. For an estimation of this cell loss according to cell type, we
190 immunostained crista receptors with antibodies against secreted phosphoprotein 1 (SPP1) / osteopontin,
191 CASPR1 and calretinin. HCI were identified by SPP1 label (Burns et al., 2015; McInturff et al., 2018; Maroto et al.,
192 2021b), while the main population of HCII was identified by the calretinin+ label. As shown in Fig. 4, the number
193 of HCI was greatly reduced after two daily injections of streptomycin ($F[4,26]=84.6$; $p<0.001$) while the number
194 of HCII was unchanged ($F[4,26]=1.45$, $p=0.25$). The loss of HCI was similar in the three groups of rats treated with
195 streptomycin (STR-300x2, STR-350x2, STR-400x2), and no recovery in HCI counts was recorded in the washout
196 group.

197 **Calyceal junction dismantlement, afferent fragmentation and synaptic loss after sub-chronic streptomycin**
198 **exposure.**

199 In addition to HCI loss, rats exposed to sub-chronic streptomycin displayed alterations in the remaining HCIs and
200 their afferents. In rats exposed to streptomycin once a day (STR-500), a reversible loss of CASPR1 fluorescence
201 occurred in the calyces contacting the surviving HCIs (Fig.5). To assess this effect, we measured the amount of
202 CASPR1 fluorescence associated with the remaining individual calyx units. The loss and recovery in the CASPR1
203 label was found across the three epithelia and in both central/striolar and peripheral zones. All ANOVA
204 comparisons resulted in significant differences (all $F[3, 19 \text{ to } 27] > 5.3$, all $p's<0.006$). As shown in Fig. 5, the
205 confocal microscope images also revealed a reversible decrease in MYO7A fluorescence intensity in the HCs of
206 the STR-500 animals. This effect was quantified in a subset of samples and significant group differences were
207 found ($F[2,11]=5.0$, $p=0.029$). The post-hoc analysis confirmed that the label (in arbitrary units) was reduced
208 from 9583 $\pm$ 1290 ($X\pm SE$, n=5) in CTRL animals to 6232 + 781 (n=4) in STR-500 (8 wk) animals ($p<0.05$, Duncan's
209 test), and recovered (10522 $\pm$ 621, n=5) after washout. In animals given two injections a day of streptomycin,
210 the intensity of CASPR1 immunoreactivity in the calyces contacting surviving HCI was also reduced by
211 streptomycin (Suppl. Fig. S6).

212 We also evaluated whether sub-chronic streptomycin altered the distribution of the potassium channel, KCNQ4,
213 in the calyx membrane, as occurs in CASP1-KO mice (Sousa et al., 2009) and in rats exposed to sub-chronic IDPN
214 (Sedó-Cabezón et al., 2015). The data, shown in Fig. 6, indicated that CASPR1 loss associates with KCNQ4
215 redistribution in the calyces of the STR-500 rats. In control rats, the KCNQ4 label is found almost exclusively in
216 the inner membrane of the calyces, that is, in the calyceal junction area. After streptomycin treatment, the
217 immunofluorescence was reduced in this location, whereas significant label appeared in the outer side of the
218 calyx. ANOVA analyses of the amount of fluorescence in the inner and outer membranes were significant ($F[3,$
219 $14]=12.1$, $P<0.001$, and $F[3,14]=49.9$, $p<0.001$, respectively). Post-hoc analyses confirmed that streptomycin
220 caused KCNQ4 redistribution, and that this effect was no longer present in the washout animals.

221 Sub-chronic streptomycin also caused a reduction in the number of synaptic puncta as revealed by labelling with
222 antibodies against ribeye/CtBP2, the core protein of the presynaptic ribbon, and against the post-synaptic

223 scaffold protein PSD-95 (post-synaptic density 95). The mean number of puncta counts per cell in 2.6 μm thick
224 sections of HCs was significantly reduced in STR-500 animals exposed for 6 weeks compared to CTRL animals
225 (Fig. 7). T-test comparisons resulted in $p < 0.001$, $p=0.018$ and $p=0.001$ for ribeye, PSD-95 and co-localization
226 values, respectively.

227 The effect of of sub-chronic streptomycin on the calyceal junction was also studied at the ultrastructural level by
228 TEM observation of samples from control rats (4 lateral crista, 2 saccules, 1 utricle), STR-500 rats exposed for 6
229 (5 lateral crista) or 8 (4 lateral crista) weeks, and STR-300x2 rats exposed for 6 weeks (3 saccules and 1 utricle).
230 In control specimens, calyceal junctions were prominent, with virtually no exception, in the two basal thirds of
231 the contact between HCI and its afferent calyx (Fig. 8A,C). This junction consist of highly electrodense pre- and
232 post-synaptic membranes, a highly regular inter-membrane distance, and electrodense extracellular space. In
233 contrast, many calyceal units in the streptomycin rats showed from fragmented, only partial, to absent junction
234 (Fig. 8B, D-F). In these units, the membrane density was similar to that of regular membranes and the area
235 displayed a more-variable inter-membrane distance, as well as a reduced extracellular electrodensity. In
236 addition, fragmented calyces were also identified in the samples from the treated animals, and these showed
237 absence of the calyceal junction (Fig. 8E, F). No fragmented calyces were observed in the control epithelia.

238 **Hair cell extrusion after sub-chronic streptomycin exposure.**

239 The occurrence of HC extrusion was evaluated by immunofluorescent analysis in samples from animals exposed
240 to streptomycin twice a day. The MYO7A and CASPR1 antibodies were combined with an anti-radixin antibody to
241 label the apical microvilli of the supporting cells and thus outline the surface of the epithelium. Images indicating
242 HC extrusion were not obtained in most sections of the crista (n=4 CTRL, 7 STR-300x2, 4 STR-350x2, and 4 STR-
243 400x2) and saccule (n=2 CTRL, 7 STR-300x2, 5 STR-350x2, and 6 STR-400x2). However, as illustrated in Fig. 9A,
244 protruding/extruding HCs were a common finding in the majority of sections of utricles from animals exposed to
245 STR-300x2 for 6 weeks (n=7) or STR-350x2 for 4 weeks (n=5), although not in utricles from animals receiving STR-

246 400x2 for 3 weeks (n=6). Control utricles (n=2) also showed no HC extrusion. In the STR-300x2 and STR-350x2
247 utricles, the occurrence was around 1-3 protruding/extruding HC per section (130-190 μm long, 25 μm thick).

248 To corroborate that the extruding MYO7A+ profiles found in the immunofluorescent analyses corresponded to
249 living HCs, we examined two utricles by TEM. As shown in Fig. 9B-C, the extruding HC showed displacement of
250 the whole cell towards the lumen of the utricle. The ultrastructural features of the cytoplasm, organelles and
251 nucleus indicated a continued activity of the cell.

252 **Occurrence of calyceal junction dismantlement in human vestibular epithelia.**

253 To evaluate whether calyceal junction dismantlement also occurs in human vestibular epithelia under stress, we
254 studied samples from patients submitted to therapeutic labyrinthectomy or translabyrinthine tumour excision.
255 The vestibular epithelia were immunolabeled with anti-CASPR1 antibodies combined with a variety of other
256 antibodies, and a total of 29 samples yielded useful information. MYO7A, calretinin and CASPR1 labels matched
257 the labelling features described above in rat samples. Also, when tested together (n=9), CASPR1 and the
258 extracellular matrix protein tenascin-C were found to localise together in the calyceal junction area, as described
259 previously in rodent samples (Lysakowski et al., 2011; Sedó-Cabezón et al., 2015; Greguske et al., 2019). In
260 contrast, the observed label of HCI by SPP1 was unreliable in the tested conditions. Among the 29 epithelia, HC
261 densities varied from high, similar to that observed in samples from control rats, to almost null. Reduced HC
262 density could result from both the patient's age and vestibular pathology; the evaluation of this pathology was
263 beyond the scope of the present study. Regarding the calyceal junctions, 18 samples were evaluated to have
264 intact or most likely intact CASPR1-labelled calyces. These included 2/2 cases of Ménière's Disease (Fig. 10A), 4/4
265 cases of meningioma (Fig.10B, C), 1/1 case of endolymphatic sac tumour and 11/22 cases of vestibular
266 schwannoma. Two other samples displayed very few HCs, with no or only one CASPR1+, hampering the
267 achievement of any conclusion on calyceal junctions. However, 9 of the samples, all of them from vestibular
268 schwannoma patients, provided images suggesting that an active process of calyx junction dismantlement was

269 taking place. This included calyces with patched CASPR1 label (Fig 10D, E) and lack of CASPR1 in calyx-only units

270 (Fig. 10F). The patched feature of the label in some calyx units was confirmed in 3D reconstructions (Suppl. Fig.

271 S7).

272 **DISCUSSION**

273 Previous work from our laboratory in rats and mice has demonstrated that sub-chronic IDPN exposure cause
274 vestibular HC extrusion, and that the extrusion is preceded by reversible calyceal junction dismantlement and
275 synaptic uncoupling (Seoane et al., 2001a; Sedó-Cabezón et al., 2015; Greguske et al., 2019). These phenomena
276 have received little research attention despite its potential relevance. HC extrusion is the main form of HC
277 demise in birds and amphibians (Hirose et al., 1999; Rubel et al., 2013) and has been sporadically observed in
278 mammalian vestibular epithelia (Li et al., 1995; Nakagawa et al., 1997; Granados and Meza, 2005). In the present
279 work, we first aimed at establishing a new rat model of sub-chronic aminoglycoside toxicity to determine
280 whether HC detachment and extrusion occur in ototoxic conditions of clinical relevance. The data obtained
281 demonstrate that the calyx junction reversibly dismantles during subchronic streptomycin exposure, in
282 association with reversible vestibular dysfunction. Synaptic uncoupling and HC extrusion were also recorded in
283 these rats. In addition, we also collected evidence indicating that calyceal junction dismantlement may take
284 place in the human vestibular system.

285 HC degeneration is effectively achieved by direct exposure to aminoglycoside antibiotics as done by trans-
286 tympanic administration or in *in vitro* studies (Kohonen and Tarkkanen, 1969; Anniko et al., 1982). However, the
287 use of more natural *in vivo* approaches to induce inner ear toxicity in laboratory animals with aminoglycosides
288 has been a challenging issue, as acute systemic intoxication may not cause ototoxic effects until the dose is large
289 enough to trigger animal death (Wu et al., 2001; Murillo-Cuesta et al., 2010). Nevertheless, several studies have
290 succeeded in establishing dosing regimes that elicit ototoxic effects with limited lethality and systemic toxicity.
291 Yet, many of these studies favour cochlear versus vestibular toxicity (Sullivan et al., 1987) or are designed to
292 accelerate the progression of the damage (Taylor et al., 2008; Oesterle et al., 2008). In the present study, we
293 successfully caused slowly progressing ototoxicity with streptomycin in young rats. By means of one daily
294 injection, significant loss of vestibular function occurred after four weeks of the highest tolerated dose, while
295 the use of two injections per day accelerated this loss in a dose-dependent manner, allowing the study of the

296 ototoxicity developing after 2-3 weeks of treatment. Interestingly, the effects were similar in both sexes and low
297 variability was recorded within groups. Thus, as similarly reported for cochlear kanamycin toxicity in rats and
298 mice (Wu et al., 2001; Jiang et al., 2006) exposure of Long-Evans rats to one or two daily doses of streptomycin
299 reliably cause vestibular toxicity. Comparing the two models, it appears that the one daily dose regimen reaches
300 a limit in its effect, while the two dose regimen seems to provide a more flexible model to study dose- and time-
301 dependent effects.

302 Streptomycin exposure in rats caused loss of HCs, deeper after two daily doses than after one dose, as revealed
303 by the SEM studies and quantified in immunofluorescence studies. Separate counts of HCI and HCII revealed
304 that the HC loss concentrated on the HCI, while HCII were spared in both injection paradigms. To identify HCI we
305 used two different markers, CASPR1 and SPP1. CASPR1 is not expressed by HCIs but is found in the membrane of
306 the calyx afferent contacting the HCI (Sousa et al., 2009; Lysakowski et al., 2011; Sedó-Cabezón et al., 2015).
307 Although streptomycin caused a specific loss of CASPR1, traces of CASPR1 label in contact with cell profiles
308 positive for Myo7a+ and negative for calretinin (see Fig 3Ab) allowed a reliable identification of HCI in the one
309 dose samples. Also, except for a minor recovery in HCI numbers in the periphery of utricles and cristas, no
310 increase in HCI numbers was found in the samples of the washout animals, in which a good recovery in CASPR1
311 expression had occurred. In addition, the loss of HCI was confirmed using a positive HCI marker, SPP1 (McInturff
312 et al., 2018), to evaluate the samples from the two daily injections experiment. To identify HCII, we also used a
313 positive marker, calretinin, and found that the number of HCII per image was not reduced in any of the two
314 exposure paradigms. Because of the method used, we can not completely exclude that a small loss of HCII was
315 masked by tissue shrinkage, but in any case this maintenance of HCII numbers per image contrasts with the
316 significant loss of HCI. While the greater sensitivity of HCI respect to HCII to ototoxic insult is widely recognized,
317 not many studies are available providing a quantitative assessment of this difference *in vivo* (Lopez et al., 1997;
318 Nakayama et al., 1996 ; Hirvonen et al., 2005; Maroto et al., 2021a).

319 The data collected add to the existing evidence that HC extrusion is a significant form of HC demise induced by
320 aminoglycosides in the mammalian vestibular system *in vivo*, as reported in the vestibular epithelia of rodents
321 exposed to other aminoglycosides using relatively long exposure paradigms (Li et al., 1995; Granados and Meza,
322 2005). Also, the present data demonstrate that calyceal junction dismantlement and synaptic uncoupling occur
323 after streptomycin, as previously demonstrated for sub-chronic IDPN (Sedó-Cabezón et al., 2015; Greguske et
324 al., 2019). The streptomycin effect includes CASPR1 down-regulation, redistribution of KCNQ4, loss of electronic
325 density in the calyceal junction area, and a reduction in the number of synaptic puncta per cell. As in the IDPN
326 model, these effects associated with loss of vestibular function, and significant recovery was recorded for the
327 behavioural, CASPR1 and KCNQ4 effects in rats allowed a washout period after the exposure. However,
328 significant differences between the two models were noticed. In the rat IDPN model (Seoane et al., 2001a; Sedó-
329 Cabezón et al., 2015), a complete dismantlement of the calyceal junctions, with extensive loss of CASPR1 and
330 redistribution of KCNQ4, occurs before HC loss starts. Extending the time of IDPN exposure triggers a massive HC
331 extrusion, and the occurrence of extruding cells over several weeks indicates that the extrusion of each HC takes
332 place over several days. IDPN thus provide a highly synchronic and slowly progressing model of sequential HC
333 detachment and extrusion. In contrast, in the streptomycin rats, extruding HC were only found occasionally, the
334 loss of CASPR1 and the redistribution of KCNQ4 were smaller, and a significant loss of HCs had occurred already
335 before complete dismantlement of the calyceal junctions. These observations indicate that, in comparison to
336 those of IDPN, the effects of streptomycin are less synchronic, and that the extrusion of each HC takes place in a
337 shorter time, probably a few hours. Although not specifically addressed in the present experiments, the TEM
338 studies did not give evidence for an extensive occurrence of apoptotic HC death. The simplest explanation of the
339 present observations is that HC detachment and extrusion is triggered at the individual cell level, and that cells
340 are not synchronized after streptomycin treatment as they are after IDPN. This conclusion is supported by our
341 previous demonstration that the calyceal junction dismantlement is triggered individually in a calyx-to-calyx
342 basis also after IDPN (Sedó-Cabezón et al., 2015).

343 Behavioural and CASPR1 data presented here demonstrate repair capacity and functional recovery of the rat
344 vestibular epithelium after sub-chronic streptomycin exposure. Although only a limited number of animals were
345 allowed to survive, their recovery was indubitable. Functional recovery may be consequent to behavioural
346 compensation or reflect recovery from alterations no detected by histological analyses, such as hypothetical
347 changes in endolymph composition or inactivation of the transduction channels. Conversely, our data excluded
348 the possibility that HC regeneration accounted for this recovery, because HCI counts remained decreased at the
349 end of the washout period. Rather, its association with the reversal in CASPR1 label, as measured on a cell-by-
350 cell basis, suggests that the functional recovery may result, at least in part, from repair phenomena in the HC
351 and the contact between HCs and their afferents. The present observation of recovery in CASPR1 label contrast
352 with the persistence of calyceal pathology observed in chinchillas exposed to gentamicin by direct perilymphatic
353 infusion (Sultemeier and Hoffman, 2017). Differences in species, aminoglycoside and exposure model may
354 account for the difference between the present data and those by Sultemeier and Hoffman (2017).

355 To explore the possible relevance of the calyceal junction dismantlement to human pathology, we examined a
356 series of human samples for histological evidence of such dismantlement. The interpretation of the human
357 observations is weakened by the lack of control samples, and the variability in pathological conditions and
358 surgery-generated damages. Nevertheless, many samples included a uniform CASPR1 label in all observable
359 calyx units, while some other samples offered multiple images of patched or largely missing label for this
360 protein. Although the possibility that this abnormality was generated during collection of the sample cannot be
361 completely excluded, the data strongly suggest that calyceal junction dismantlement may indeed occur in the
362 human vestibule under stressful conditions. Although all the cases in which CASPR1 loss was recorded were
363 cases of vestibular schwannoma, the number of samples from other pathologies was so low that it cannot be
364 discarded that similar observations could emerge if more cases were examined. Current evidence indicates that
365 vestibular schwannomas may damage the sensory epithelia of the inner ear through tumour-secreted factors,
366 including tumour necrosis factor alpha (TNFα) (Dilwali et al., 2015). A recent study has demonstrated the

367 potential of this pro-inflammatory cytokine to cause cochlear synaptic uncoupling *in vivo* (Katsumi et al., 2020).
368 It is thus possible that inflammatory signals like TNFα are able to trigger the dismantlement of the calyceal
369 junction, synaptic uncoupling, and eventually HC extrusion in the vestibular epithelium.

370 In conclusion, the present study evaluate whether events leading to HC extrusion in the vestibular sensory
371 epithelia of rodents exposed to sub-chronic IDPN may have a wider significance. The data collected demonstrate
372 that dismantlement of the calyceal junction and synaptic uncoupling are widespread phenomena in rats exposed
373 to sub-chronic streptomycin regimes that cause HC loss through, at least in part, the extrusion pathway. We also
374 collected data suggesting that calyceal junction dismantlement may occur in human vestibular epithelia in
375 response to inflammatory stress. Elucidating the molecular pathways triggering these cellular phenomena may
376 unveil new targets to control damage progression in this sensory epithelium.

377 **MATERIALS AND METHODS**

378 **Animals and treatments**

379 Animals were used in accordance with Law 5/1995 and Act 214/1997 of the Generalitat de Catalunya and
380 approved by the University of Barcelona's Ethics Committee on Animal Experiments and the Commission on
381 Animal Experimentation of the Generalitat. Long-Evans rats were obtained from Janvier Labs (Le-Genest-Saint-
382 Isle, France) at post-natal day 8-12. They were housed with lactating mothers in standard Macrolon cages
383 (215×465×145 mm) with wood shavings as bedding. At day 21, the rats were weaned and housed in groups of
384 four of the same sex. Housing conditions included a 12:12 h light:dark cycle (07:30-19:30 h), a 22±2°C room
385 temperature and an *ad libitum* access to standard pellet diets (TEKLAD 2014, Harlan Laboratories, Sant Feliu de
386 Codines, Spain).

387 A total of 98 rats (58 males, 40 females) were used in two different administration protocols, one injection per
388 day and two injections per day. The first administration protocol was designed on the grounds of the protocols
389 by Granados and Meza, 2005, and Schirmer et al., 2007. Animals were administered streptomycin sulphate salt
390 (Sigma-Aldrich, S6501), s.c., dissolved in PBS, starting at postnatal 21, daily for 6 or 8 weeks. To ensure dose
391 accuracy, injection volumes were 10 ml/kg at the beginning, but were reduced to 2 ml/kg as the rats increased
392 body weights. Different injection sites in the dorsal skin were used in an alternating sequence. In this first series
393 of experiments, rats were dosed with 0 (control vehicle), 100, 300, 400 or 500 mg/kg · day of streptomycin
394 (referred to the free base), once a day, for 6 or 8 weeks. Two experimental batches used only males, one only
395 females, and the fourth included an equal number of males and females. Acute toxicity and lethality is described
396 in the results section above. A final experiment used a second administration protocol, in which the total daily
397 dose was split into two injections given 8 h apart. This dosing paradigm was designed to evaluate the vestibular
398 effects of larger daily doses and circumvent the acute toxicity of streptomycin recorded in rats receiving the 500
399 mg/kg dose. Thus, rats received 0, 600, 700 or 800 mg/kg · day in two daily doses of 0, 300 mg/kg (for 6 weeks),

400 350 mg/kg (for 4 weeks) or 400 mg/kg (for 3 weeks). No animals died in this experiment. The detail of all groups
401 of animals used is shown in Supplementary Table S1.

402 During the period of treatment, the animals were weighted and assessed for wellbeing daily. They were also
403 tested for vestibular function once a week. At the end of the treatment period, some animals were allowed to
404 survive for up to 8-10 additional weeks to evaluate the potential reversibility of the vestibular dysfunction and
405 the histopathological effects of streptomycin. Some control animals were also allowed to survive the recovery
406 period to provide control body weight and vestibular function data. The day after that of the last dose, or after
407 the period of recovery, rats were euthanized by decapitation under anaesthesia. The skull was sectioned in half
408 and placed in fixative solution under a fume hood for dissection of the vestibular sensory epithelia. The epithelia
409 from the first ear were typically obtained within 5 min after decapitation and used for scanning (SEM) and
410 transmission (TEM) electron microscopy. The epithelia from the second ear, obtained within 15 min after
411 decapitation were used for immunohistochemistry. Some animals were used for immunohistochemistry only.

412 **Human samples**

413 Vestibular sensory epithelia were collected from patients submitted to therapeutic labyrinthectomy or
414 translabyrinthine tumour excision. The samples included in the study, detailed in Supplementary Table S2, are
415 from 2 cases of Ménière's Disease, 1 case of endolymphatic sac tumour, 4 cases of meningioma, and 22 cases of
416 vestibular schwannoma. Patients were 18 to 70 years old, and 54 % were females. The tissues were obtained
417 after informed consent, as approved by the Clinical Ethics Committee of the Hospital Germans Trias i Pujol. The
418 samples were placed in formalin and sent to the laboratory, usually in 24 h, although some samples were
419 delayed for up to 8 days. The tissues were then rinsed in phosphate buffered saline (PBS, pH 7.2), transferred
420 into a cryoprotective solution (34.5% glycerol, 30% ethylene glycol, 20% PBS, 15.5% distilled water) and stored
421 at -20ºC until further processing.

422 **Assessment of vestibular function in rats**

423 To evaluate vestibular function, we assessed the tail-lift reflex as described (Martins-Lopes et al., 2019; Maroto
424 et al., 2021 a,b). Briefly, rats are held by the base of the tail and quickly but gently lifted upwards to
425 approximately 40 cm above ground and immediately returned down. In healthy rats, this triggers a trunk and
426 limbs extension reflex in a landing response. Loss of vestibular function results in loss of the anti-gravity
427 extension reflex, so the rat curls ventrally (Hunt et al., 1987; Pellis et al., 1991; Llorens et al., 1991; Maroto et al.,
428 2021c). The reflex response of the animal is recorded from the side with high-speed video (we use 240 frames
429 per second with a GoPro 5 camera) and the records are used to obtain the minimum angle formed by the nose,
430 the back of the neck and the base of the tail during the tail-lift manoeuvre (tail-lift angle, TLA), as described
431 (Martins-Lopes et al., 2019; Maroto et al., 2021a,c). The TLA has been demonstrated to provide an objective
432 measure of permanent or reversible vestibular loss (Martins-Lopes et al., 2019; Maroto et al., 2021a,c).

433 **Electron microscopy**

434 For SEM and TEM, rat vestibular epithelia were dissected in 2.5% glutaraldehyde in 0.1 M cacodylate buffer (pH
435 7.2), and fixed overnight in this solution. The epithelia were then rinsed with cacodylate buffer, post-fixed for 1
436 h in 1% osmium tetroxide in the same buffer, rinsed again and stored in 70% ethanol at 4ºC until further
437 processing. Afterwards, the samples were dehydrated with increasing concentrations of ethanol, up to 100%.
438 For TEM analysis, the lateral crista was embedded in Spurr resin. To select the level of interest, semi-thin
439 sections (1 µm) were stained with 1% toluidine blue and examined in a light microscope. Ultrathin sections were
440 stained with uranyl acetate and lead citrate and were observed with a JEOL 1010 microscope at 75-80 kV. For
441 SEM analysis of epithelial surfaces, the dehydrated specimens were dried in a Polaron E3000 critical-point dryer
442 using liquid CO2, coated with carbon, and observed in a JEOL JSM-7001F field emission SEM.

443 **Immunohistochemistry**

444 The following commercial primary antibodies were used: mouse monoclonal anti-CASPR1 (clone K65/35; used at
445 1:400 dilution) and anti-PSD95 (clone K28/43, 1:100) from the UC Davis / NIH NeuroMab Facility; mouse

446 monoclonal anti-Ribeye/CtBP2 (clone 16/CtBP2, BD Transduction Labs, 1:100); rabbit anti-myosin VIIa (25-6790,
447 Proteus Biosciences; 1:400); guinea pig anti-calretinin (214.104, Synaptic Systems, 1/500); goat anti-SPP1
448 (AF808, RD systems, 1/200). We also used a rabbit anti-KCNQ4 (PB-180, 1/1000) donated by Bechara Kachar
449 (National Institute on Deafness and Other Communication Disorders, NIH; Beisel et al., 2005). To reveal the
450 primary antibodies, we used Day-Light-405, Alex-488, Alexa-555 and Alexa-647-conjugated secondary antibodies
451 from Invitrogen / Thermo Fisher. To image synaptic puncta, we used isotype-specific secondary antibodies, i.e.,
452 anti-mouse-IgG1 to reveal the Ribeye/CtBP2 antibody and anti-mouse IgG2a to reveal the PSD-95 antibody.

453 After dissection, the rat vestibular epithelia were fixed for 1 h at room temperature in 4 % paraformaldehyde in
454 PBS. These samples were rinsed in PBS, transferred into the cryoprotective solution and stored at -20ºC. To
455 circumvent potential bias from batch-to-batch differences in immunolabelling, we processed in parallel
456 specimens from each experimental group. For immunolabelling, rat or human tissues were washed with PBS to
457 remove the cryoprotective solution, permeated in 4% Triton-X-100 in PBS for 1 h at room temperature, and then
458 blocked in 0.5% Triton-X-100 and 1% fish gelatine in PBS (Sigma-Aldrich, cat.# G7765) also for 1 h at room
459 temperature. They were then incubated with the mixed primary antibodies in 0.1% Triton-X-100 and 1% fish
460 gelatine in PBS for 24 h at 4ºC, followed by incubation with the secondary antibodies in the same conditions.
461 The samples were thoroughly rinsed with PBS following each incubation and gently rocked during the
462 incubations and washes. The immunolabelled epithelia were whole-mounted in Mowiol medium, or sectioned
463 before mounting in the same medium. To obtain sections, the tissues were embedded in a mixture of 0.49%
464 gelatin, 30% bovine serum albumin, and 20% sucrose in PBS overnight at 4 ºC. This same medium was used to
465 form a block by solidification with 2 % glutaraldehyde, one sample placed oriented in its surface, and a second
466 block formed on top of it. Using a Leica VT1000S vibrating microtome, sections of 40 μm were obtained from
467 this layered block with the specimen placed in between the two halves. A detailed version of this protocol has
468 been published (Maroto et al., 2021b).

469 **Confocal microscopy observation and analysis**

470 Tissue sections were observed in a Zeiss LSM880 spectral confocal microscope. In animal studies, image
471 acquisition settings were maintained across samples from each immunolabelling batch. To obtain HC counts, Z-
472 stacks of 0.5 μm thick optical sections were obtained spanning 25 μm with the 63X objective. Then, 3 μm thick
473 images were obtained by projecting 6-by-6 consecutive images from the stack. The ImageJ software (National
474 Institute of Mental Health, Bethesda, Maryland, USA) was used for quantitative image analyses. Epithelia of
475 animals injected once a day with streptomycin were labelled with anti-MYO7A, anti-CASPR1, and anti-calretinin
476 antibodies. HCI were defined as MYO7A+ cells surrounded by a calyceal CASPR1+ label, even in cases where this
477 label appeared thin and fragmented. HCII were defined as cells labelled with both the anti-MYO7A and anti-
478 calretinin antibodies. MYO7A+ cells not identified as HCI or HCII by the respective CASPR1 or calretinin labels (3-
479 6 %) were excluded from the analysis. For each animal and epithelial zone, the number of cells was obtained by
480 averaging counts from 8 different areas. To evaluate the loss of CASPR1 label in the calyces, the amount of
481 fluorescence in the corresponding colour channel was measures in individual calyceal units using a 100 μm^2
482 region of interest on a single optical section. An average estimate was obtained for each epithelium and zone of
483 each animal, and the statistical analysis was performed to compare among groups of animals. To compare the
484 distribution of KCNQ4 in the inner and outer membranes of the calyx, we assessed the profile of fluorescence
485 intensity along a line drawn across the calyx as described (Sousa et al., 2009; Sedó-Cabezón et al., 2015). To
486 evaluate synaptic elements, 2.6 μm thick optic sections were used to determine the number of presynaptic
487 Ribeye/CtBP2 puncta, postsynaptic PSD95 puncta, as well as the Ribeye-PSD95 co-localization, in HCs in which
488 the nucleus extended top to bottom of the optical section.

489 **Data analysis**

490 Data show mean +/- standard error of the mean except where indicated. Body weight and behavioural data
491 were analysed with repeated-measures MANOVA (Wilks' criterion) with the day as the within-subject factor.
492 Day-by-day analysis was performed after significant day-by treatment interactions were recorded. Other data

493 were analysed by appropriate ANOVA designs and Duncan's post-hoc test, or by Student's t-test. The IBM SPSS

494 Statistics 25 program package was used.

495 **REFERENCES**

496 Anniko, M., Takada, A. and Schacht, J. (1982) Comparative ototoxicities of gentamicin and netilmicin in three
497 model systems. *Am. J. Otolaryngol*. 3, 422-33.

498 Beisel, K.W., Rocha-Sanchez, S.M., Morris, K.A., Nie, L., Feng, F., Kachar, B., Yamoah, E.N. and Fritzsch, B (2005)
499 Differential expression of KCNQ4 in inner hair cells and sensory neurons is the basis of progressive high-
500 frequency hearing loss. *J. Neurosci.* 25, 9285–9293.

501 Benkafadar, N., Janesick, A., Scheibinger, M., Ling, A. H., Jan, T. A. and Heller, S. (2021). Transcriptomic
502 characterization of dying hair cells in the avian cochlea. *Cell Rep.* 34, 108902. doi:
503 10.1016/j.celrep.2021.108902

504 Black, F.O., Gianna-Poulin, C. and Pesznecker, S.C. (2001). Recovery from vestibular ototoxicity. *Otol. Neurotol.*
505 22, 662-671.

506 Black, F.O., Pesznecker, S. and Stallings, V. (2004). Permanent gentamicin vestibulotoxicity. *Otol. Neurotol.* 25,
507 559-569.

508 Burns, J. C., Kelly, M. C., Hoa, M., Morell, R. J. and Kelley, M. W. (2015). Single-cell RNA-Seq resolves cellular
509 complexity in sensory organs from the neonatal inner ear. *Nat. Commun.* 6, 8557. doi:
510 10.1038/ncomms9557

511 Dechesne, C.J., Winsky, L., Kim, H.N., Goping, G., Vu, T.D., Wenthold, R.J. and Jacobowitz, D.M. (1991)
512 Identification and ultrastructural localization of a calretinin-like calcium-binding protein (protein 10) in the
513 guinea pig and rat inner ear. *Brain. Res.* 560, 139-148.

514 Dilwali, S., Landegger, L. D., Soares, V. Y., Deschler, D. G. and Stankovic, K. M. (2015). Secreted factors from
515 human vestibular schwannomas can cause cochlear damage. *Sci. Rep.* 5, 18599. doi: 10.1038/srep18599

516 Furness, D.N. (2015). Molecular basis of hair cell loss. *Cell Tissue Res.* 361, 387-399.

517 Granados, O. and Meza, G. (2005). Streptidine, a metabolic derivative produced after administration of
518 streptomycin in vivo, is vestibulotoxic in rats. *Histol. Histopathol*. 20, 357-364.

519 Greguske, E.A., Carreres-Pons, M., Cutillas, B., Boadas-Vaello, P. and Llorens, J. (2019) Calyx junction
520 dismantlement and synaptic uncoupling precede hair cell extrusion in the vestibular sensory epithelium
521 during sub-chronic 3,3'-iminodipropionitrile ototoxicity in the mouse. *Arch. Toxicol.* 93, 417-434.

522 Hasson, T., Gillespie, P.G., Garcia, J.A., MacDonald, R.B., Zhao, Y., Yee, A.G., Mooseker, M.S., Corey, D.P. (1997)
523 Unconventional myosins in inner-ear sensory epithelia. *J. Cell. Biol.* 137, 1287-1307.

524 Hirose, K., Westrum, L.E., Stone, J.S., Zirpel, L. and Rubel, E.W. (1999) Dynamic studies of ototoxicity in mature
525 avian auditory epithelium. *Ann. N.Y. Acad. Sci*. 884, 389-409.

526 Hirvonen, T.P., Minor, L.B., Hullar, T.E. and Carey, J.P. (2005). Effects of intratympanic gentamicin on vestibular
527 afferents and hair cells in the chinchilla. *J. Neurophysiol*. 93, 643-655.

528 Hunt, M.A., Miller, S.W., Nielson, H.C. and Horn, K.M. (1987) Intratympanic injections of sodium arsanilate
529 (atoxil) solution results in postural changes consistent with changes described for labyrinthectomized rats.
530 *Behav. Neurosci.* 101, 427–428.

531 Jiang, H., Sha, S. H., Forge, A. and Schacht, J. (2006). Caspase-independent pathways of hair cell death induced
532 by kanamycin in vivo. *Cell Death Differ.* 13, 20–30.

533 Katsumi, S., Sahin, M. I., Lewis, R. M., Iyer, J. S., Landegger, L. D., & Stankovic, K. M. (2020). Intracochlear
534 perfusion of tumor necrosis factor-alpha induces sensorineural hearing loss and synaptic degeneration in
535 guinea pigs. *Front. Neurol.* 10, 1353.

536 Kohonen, A. and Tarkkanen, J. (1969) Cochlear damage from ototoxic antibiotics by intratympanic application.
537 *Acta Otolaryngol.* 68, 90-97.

538 Li, L., Nevill, G. and Forge, A. (1995). Two modes of hair cell loss from the vestibular sensory epithelia of the
539 guinea pig inner ear. *J. Comp. Neurol*. 355, 405-417.

540 Llorens, J. and Rodríguez-Farré, E. (1997). Comparison of behavioral, vestibular, and axonal effects of subchronic
541 IDPN in the rat. *Neurotoxicol. Teratol*. 19, 117-127.

542 Llorens, J., Demêmes, D. and Sans, A. (1993). The behavioral syndrome caused by 3,3'-iminodipropionitrile and
543 related nitriles in the rat is associated with degeneration of the vestibular sensory hair cells. *Toxicol. Appl.*
544 *Pharmacol*. 123, 199-210.

545 Lopez, I., Honrubia, V., Lee, S.C., Schoeman, G. and Beykirch, K. (1997) Quantification of the process of hair cell
546 loss and recovery in the chinchilla crista ampullaris after gentamicin treatment. *Int. J. Dev. Neurosci.* 15,
547 447-461.

548 Lopez-Escamez, J.A., Carey, J., Chung, W.H., Goebel, J.A., Magnusson, M., Mandala, M., Newman-Toker, D.E.,
549 Strupp, M., Suzuki, M., Trabalzini, F. and Bisdorff, A. (2015) Diagnostic criteria for Menière's disease. *J.*
550 *Vestib. Res.* 25, 1-7.

551 Lysakowski, A., Gaboyard-Niay, S., Calin-Jageman, I., Chatlani, S., Price, S.D. and Eatock, R.A. (2011). Molecular
552 microdomains in a sensory terminal, the vestibular calyx ending. *J. Neurosci*. 31, 10101–10114.

553 Maroto, A. F., Barrallo-Gimeno, A. and Llorens, J. (2021a). Relationship between vestibular hair cell loss and
554 deficits in two anti-gravity reflexes in the rat. Hear. Res. 410, 108336. doi: 10.1016/j.heares.2021.108336

555 Maroto, A.F., Greguske, E.A., Barrallo-Gimeno, A. and Llorens, J. (2021b) Evaluation of cellular and molecular
556 pathology in the rodent vestibular sensory epithelia by immunofluorescent staining and confocal
557 microscopy. In: E*xperimental Neurotoxicology Methods, Neuromethods, vol. 172*, Llorens, J. and Barenys.
558 M., Editors. Springer US, pp 35-50.

559 Maroto, A.F., Greguske, E.A., Deulofeu, M., Boadas-Vaello, P. and Llorens, J. (2021c) Behavioral assessment of
560 vestibular dysfunction in rats. In: E*xperimental Neurotoxicology Methods, Neuromethods, vol. 172*, Llorens,
561 J. and Barenys. M., Editors. Springer US, pp 199-215.

562 Martins-Lopes, V., Bellmunt, A., Greguske, E.A., Maroto, A.F., Boadas-Vaello, P. and Llorens, J. (2019)
563 Quantitative assessment of anti-gravity reflexes to evaluate vestibular dysfunction in rats. *J. Assoc. Res.*
564 *Otolaryngol.* 20, 553-563.

565 McInturff, S., Burns, J.C., Kelley, M.W. (2018) Characterization of spatial and temporal development of Type I
566 and Type II hair cells in the mouse utricle using new cell-type-specific markers. *Biol. Open* 7, bio038083.
567 doi: 10.1242/bio.038083.

568 Murillo-Cuesta, S., Contreras, J., Cediel, R. and Varela-Nieto, I. (2010) Comparison of different aminoglycoside
569 antibiotic treatments to refine ototoxicity studies in adult mice. *Lab. Anim.* 44, 124-131.

570 Nakagawa, T., Yamane, H., Shibata, S. and Nakai, Y. (1997) Gentamicin ototoxicity induced apoptosis of the
571 vestibular hair cells of guinea pigs. *Eur. Arch. Otorhinolaryngol.* 254, 9-14.

572 Nakayama, M., Riggs, L.C. and Matz, G.J. (1996) Quantitative study of vestibulotoxicity induced by gentamicin or
573 cisplatin in the guinea pig. *Laryngoscope* 106, 162-167.

574 Oesterle, E.C., Campbell, S., Taylor, R.R., Forge, A. and Hume, C.R. (2008) Sox2 and JAGGED1 expression in
575 normal and drug-damaged adult mouse inner ear. *J. Assoc. Res. Otolaryngol.* 9, 65-89.

576 Pellis, S.M., Pellis, V.C. and Teitelbaum, P. (1991) Labyrinthine and other supraspinal inhibitory controls over
577 head-and-body ventroflexion. *Behav. Brain Res*. 46, 99-102.

578 Rubel, E.W., Furrer, S.A. and Stone, J.S. (2013). A brief history of hair cell regeneration research and speculations
579 on the future. *Hear Res*. 297, 42-51.

580 Sedó-Cabezón, L., Jedynak, P., Boadas-Vaello, P. and Llorens, J. (2015) Transient alteration of the vestibular
581 calyceal junction and synapse in response to chronic ototoxic insult in rats. *Dis. Model. Mech.* 8, 1323-1337.

582 Seoane, A., Demêmes, D. and Llorens, J. (2001a). Relationship between insult intensity and mode of hair cell loss
583 in the vestibular system of rats exposed to 3,3'-iminodipropionitrile. *J. Comp. Neurol.* 439, 385-399.

584 Seoane, A., Demêmes, D. and Llorens, J. (2001b). Pathology of the rat vestibular sensory epithelia during
585 subchronic 3,3'-iminodipropionitrile exposure: hair cells may not be the primary target of toxicity. *Acta*
586 *Neuropathol*. 102, 339-348.

587 Sousa, A.D., Andrade, L.R., Salles, F.T., Pillai, A.M., Buttermore, E.D., Bhat, M.A. and Kachar, B (2009). The
588 septate junction protein caspr is required for structural support and retention of KCNQ4 at calyceal synapses
589 of vestibular hair cells. *J. Neurosci*. 29, 3103-3108.

590 Sullivan, M. J., Rarey, K. E. and Conolly, R. B. (1987). Comparative ototoxicity of gentamicin in the guinea pig and
591 two strains of rats. Hear. Res. 31, 161–167.

592 Taylor, R.R., Nevill, G. and Forge, A. (2008) Rapid hair cell loss: a mouse model for cochlear lesions. *J. Assoc. Res.*
593 *Otolaryngol.* 9, 44-64.

594 von Brevern, M., Bertholon, P., Brandt, T., Fife, T., Imai, T., Nuti, D. and Newman-Toker, D. (2015) Benign
595 paroxysmal positional vertigo: Diagnostic criteria. *J. Vestib. Res.* 25, 105-117-

596 Wu, W.J., Sha, S.H., McLaren, J.D., Kawamoto, K., Raphael, Y. and Schacht, J. (2001) Aminoglycoside ototoxicity
597 in adult CBA, C57BL and BALB mice and the Sprague-Dawley rat. *Hear. Res.* 158; 165-178.

598 LEGENDS FOR FIGURES

599 **Figure 1.** Effects of sub-chronic streptomycin on the tail-lift reflex of rats. Data are mean ± SE minimum angles
600 formed by the nose, the back of the neck and the base of the tail during the reflex behaviour elicited by a tail-lift
601 manoeuvre. Loss of vestibular function causes loss of the anti-gravity trunk extension reflex, which results in
602 ventral curling and thus in smaller angles. **A.** Effects of one injection per day at 0 (CTRL, vehicle control) or 500
603 mg/kg (STR-500) of streptomycin for 6 weeks, starting at 21 days of age. * $p<0.05$, different from control group
604 after significant day by treatment interaction effect in repeated-measures MANOVA. **B.** Effects of two injections
605 per day at 0 (CTRL, vehicle control), 300 (STR-300x2), 350 (STR-350x2), or 400 (STR-400x2) mg/kg of
606 streptomycin for 6, 6, 4, or 3 weeks, respectively, starting at 21 days of age. The numbers of animals were
607 reduced to 6 in the CTRL group after day 28, and to 7 in the STR-350x2 and STR-400x2 groups after day 21. **a, b,**
608 **c, d**: groups with different letters are significantly different ($p<0.05$), Duncan's test after significant ANOVA on
609 that day. **C.** Recovery of the tail-lift reflex after the end of exposure in rats administered once a day with 500
610 mg/kg (STR-500) of streptomycin for 6 weeks. **D.** Loss and recovery of the tail-lift reflex in two individual rats
611 administered twice a day with 350 (STR-350) or 400 mg/kg (STR-400) of streptomycin for 3 weeks, followed by 3
612 weeks of washout..

613 **Figure 2.** Effects of sub-chronic streptomycin on the vestibular sensory epithelium of the rat as observed in
614 surface preparations of saccules examined by SEM. **A.** Control saccule, showing a high and uniform density of
615 stereocilia bundles throughout the macula. **B.** Effect of one injection per day of 500 mg/kg of streptomycin (STR-
616 500) for 8 weeks. A reduced density of stereocilia bundles is noticeable at this low magnification. The boxed area
617 is shown at higher magnification in panel C. **C.** Higher magnification of the saccule shown in panel B. Note the
618 areas where the lack of stereocilia bundles is evident (arrows). **D and E.** High magnification views of a saccule
619 from a STR-500 rat at 6 weeks of treatment. Note the contacts between the apical edges of supporting cells,
620 marked by a high density of microvellosities, denoting the lack of stereociliary bundles (star), and the bundles

621 showing stereocilia fusion and HC protrusion into the luminal cavity (arrows). **Scale Bars:** 100 μm in **A** and **B**; 20
622 μm in **C**; 2 μm in **D**; 5 μm in **E**.

623 **Figure 3.** Effects of sub-chronic streptomycin on the numbers of HCI and HCII in the central/striola (C/S) and
624 peripheral (P) regions of the vestibular crista, utricle and saccule, as obtained from confocal images of epithelia
625 labelled with anti-MYO7A (red), anti-CASPR1 (green) and anti-calretinin (blue) antibodies. **A**. Representative
626 images from the peripheral utricle of a control rat **(a)**, a rat treated with 500 mg/kg of streptomycin, once a day,
627 for 8 weeks **(b)**, and a rat treated with streptomycin and allowed 8 weeks of recovery after the end of the
628 treatment **(c)**. HCI were defined by MYO7A+ cells with adjacent CASPR1 label (arrows). To estimate HCIIs, we
629 counted cells with double MYO7A+ and calretinin label. Note the fragmentation of the CASPR1 label in the
630 streptomycin rat (arrows in **b**). To improve readability of the micrograph, a section in the upper right corner of
631 image **b** has been replaced by a drawn triangle. **Scale bar** in (**c**): 20 μm. **B and C.** Counts of HCI **(B)** and HCII **(C)**
632 cells. Data are mean number of cells +/- SE per section. For each animal and epithelial zone, numbers were
633 obtained by averaging counts from 8 areas. Numbers below the bars indicate number of animals included per
634 group. **a, b, c, ab, ac**: groups not sharing a letter are different ($p<0.05$), Duncan's multiple-comparisons test after
635 significant ($p<0.05$) one-way ANOVA. Absence of letters denote group comparisons that resulted in non-
636 significant differences in the ANOVA analysis.

637 **Figure 4.** Effects of sub-chronic streptomycin on HC density in the vestibular crista. Samples were from animals
638 receiving 0 (Control, CTRL), 300 (STR-300x2), 350 (STR-350x2) or 400 (STR-400x2) mg/kg of streptomycin, twice a
639 day, for 6, 4, or 3 weeks. The washout (WO) group includes animals allowed 3 weeks of recovery after receiving
640 STR-350x2 or STR-400x2 for 3 weeks. The cristae were labelled with anti-SPP1 (blue), anti-CASPR1 (green) and
641 anti-calretinin (red) antibodies. HCI were defined as SPP1+ cells and HCII were cells with calretinin label. **A.**
642 Partial view of representative sections of control and streptomycin cristae. **B.** Relative numbers of HCI and HCII
643 in the crista sections. Data are mean number of cells +/- SE per transversal section, including central and

644 peripheral regions. **a, b**: groups not sharing a letter are different ($p<0.05$), Duncan's multiple-comparisons test
645 after significant ($p<0.05$) one-way ANOVA. Comparison of HCII group means was non-significant.

646 **Figure 5.** Effects of sub-chronic streptomycin on the expression of CASPR1 in the central/striola (C/S) and
647 peripheral (P) regions of the vestibular crista, utricle and saccule of the rat. The samples were labelled with anti-
648 MYO7A (red), anti-CASPR1 (green) and anti-calretinin (blue) antibodies. **A.** Representative images from mid-
649 crista sections from a CTRL rat (**a** to **d**), a rat treated with 500 mg/kg of streptomycin, once a day, for 6 weeks (**e**
650 to **h**), and a rat allowed recovery during a washout period of 10 weeks after the streptomycin treatment (**i** to **l**).
651 Note the loss and fragmentation of the CASPR1 label caused by streptomycin and its recovery after washout.
652 The intensity of MYO7A label also decreased and recovered. **B.** Quantitative analysis of the CASPR1
653 fluorescence. Data are normalised arbitrary fluorescence amount per cell +/- SE. For each animal, epithelium
654 and zone, the average amount of fluorescence was obtained from all HCs available for analysis up to 40 cells.
655 Numbers below the bars indicate number of animals included per group. **a, b**: groups not sharing a letter are
656 different ($p<0.05$), Duncan's multiple-comparisons test after significant ($p<0.05$) one-way ANOVA.

657 **Figure 6.** Effects of sub-chronic streptomycin on the distribution of KCNQ4 in the inner and outer membrane of
658 the calyx terminals afferent to HCI in the rat. Vestibular crista were labelled with anti-CASPR1 (green) and anti-
659 KCNQ4 (red) antibodies. **A.** Image from a crista showing the redistribution of KCNQ4. The asterisk indicates a
660 calyx with a control-like co-localisation of CASPR1 and KCNQ4. The arrowhead points to a calyx with CASPR1 loss
661 and reduced co-localisation, with the KCNQ4 antibody labelling a greater area than the CASPR1 antibody. The
662 arrow points to the outer membrane of a calyx with greatly reduced CASPR1 label and redistribution of KCNQ4
663 throughout both the inner (i and i') and outer (o and o') membranes. **B.** Quantitative analysis of the distribution
664 of KCNQ4 label in the inner and outer face of the calyces in crista from control rats (CTRL), rats treated with 500
665 mg/kg of streptomycin (STR-500), once a day, for 6 weeks, and rats allowed recovery during a washout period of
666 8-10 weeks after the streptomycin treatment. Data are mean arbitrary fluorescence units +/- SE. The number of

667 replicas indicate the number of animals included in the analysis per group. **a, b**: groups not sharing a letter are
668 different ($p<0.05$), Duncan's multiple-comparisons test after significant ($p<0.05$) one-way ANOVA.

669 **Figure 7.** Effects of sub-chronic streptomycin on the numbers of synaptic puncta per 2.6 μm-tick optical sections
670 of HCs in vestibular crista labeled with anti-MYO7A, anti-ribeye and anti-PSD95 antibodies. **A.** Synaptic puncta
671 labelling. In subpanel **a**, the MYO7A label is included to show HC bodies in a control crista. Subpanel b shows the
672 same image without the MYO7A label but including lines delineating the limits of two HCs and arrows pointing
673 to examples of pairs of pre-synaptic (ribeye, red) and post-synaptic (PSD-95, green) puncta. **B.** Mean number of
674 pre-synaptic and post-synaptic puncta, as well as pre- and post-synaptic pairs, +/- SE, from control rats (CTRL)
675 and rats treated with 500 mg/kg of streptomycin (STR-500), once a day, for 6 weeks. The number of replicas
676 indicate the number of animals included in the analysis per group. *: $p< 0.05$, and ***: $p<0.001$, CTRL versus
677 STR-500, Student's T-test.

678 **Figure 8.** Effects of sub-chronic streptomycin on the calyceal junction and calyx integrity as observed by TEM. **A.**
679 Control crista. The calyceal junction is revealed by the high electron density of the apposing membranes (long
680 arrows) of HCI and inner side of the calyx (c), higher than that found in the outer side of the calyx (arrowheads).
681 **B.** Crista of a rat exposed to 500 mg/kg of streptomycin, once a day, for 6 weeks. In most of the area where the
682 calyceal junction should be found, the apposing membranes show a low electron density (short arrows), similar
683 to that in the outer face of the calyx (arrowhead). **C.** Higher magnification of the calyceal junction (long arrow)
684 and the outer side of the calyx (arrowhead) in a control saccule. **D.** Higher magnification from a crista of a rat
685 exposed to 500 mg/kg of streptomycin, once a day, for 6 weeks. Note the short segment of calyceal junction
686 (long arrow) that remains together with areas devoid of it (short arrow) and the similarity between the latter
687 and the membranes in the outer side of the calyx (arrowheads). **E.** Calyceal junction dismantlement and calyx
688 fragmentation in a HCI showing evidence of ongoing extrusion, from a utricle of a rat exposed to 300 mg/kg of
689 streptomycin, twice a day, for 6 weeks. Note the absence of calyceal junction (short arrows), the fragmentation
690 of the calyx (c, green shadow), and the direct contact between supporting cells and the HCI (stars). The purple

691 shadow highlights one supporting cell (sc). **F.** Higher magnification of the boxed area in panel **E**. Note the
692 similarity of the membranes between the place where the calyceal junction is missing (short arrows) and the
693 outer side of the calyx (arrowheads). Note also the direct contact between a supporting cell (sc) and the HCI
694 (star). **Scale Bars: A**, **B**, and **E**, 2 mm; **C**, **D**, and **F**, 1 mm.

695 **Figure 9.** Evidence of HC extrusion in utricles of rats exposed to sub-chronic streptomycin as observed by
696 immunofluorescence and TEM. The images are from rats administered twice a day with 350 mg/kg of
697 streptomycin for 4 weeks, or with 300 mg/kg for 6 weeks. **A.** Utricles immunolabeled with antibodies against
698 MYO7A (red), CASPR1 (green) and radixin (blue). The radixin label of stereocilia and microvilli outlines the
699 surface of the epithelium. Arrowheads point to HCs protruding (**a**, **b**), extruding (**c**, **d**, **e**) or completely extruded
700 (**f**) into the luminal cavity of the utricle. **B** and **C.** TEM images of HCs in a protrusion stage corresponding to that
701 shown in panels **a** and **b**, respectively, of part **A**. Stereocilia (arrows) and striated organelles (arrowheads)
702 identify the extruding cells as HCs. In **B**, note the position of the nucleus of the HC inside the epithelium, and the
703 remnant of a calyx terminal (green shadow) that identifies the HC as a HCI. In **C**, note the position of the nucleus
704 of the HC (unidentified type), half way into the luminal cavity of the utricle. **Scale Bars: A**, 20 mm; **B**, and **C**, 2
705 mm.

706 **Figure 10.** Evaluation of the calyceal junction in vestibular epithelia from patients of vestibular diseases, as
707 revealed by CASPR1 immunolabel (green, light blue when co-localizing with calretinin blue label). In the main
708 panels, HC bodies are labelled with an anti-MYO7A antibody (red). Calretinin is shown in blue in main panels **C** to
709 **F**, and in purple in the inset in **C**. **A**. Epithelium from a patient of Ménière's Disease showing no pathological
710 features. Note the elevated density of HCs and the continuous distribution of the CASPR1 label throughout the
711 calyceal junction area of each HCI. **B.** Epithelium from a meningioma patient, showing also no overt pathology.
712 **C.** Epithelium from a meningioma patient. Note the low density of HCs and the normally continuous CASPR1
713 label in calyces of both calretinin+ calyx-only terminals (arrowhead) and calretinin- dimorphic terminals (short
714 arrow). The **inset** displays the same two calyces; a thinner stack is shown to highlight the uninterrupted CASPR1

715 label and its placement in the inner membrane of the calretinin+ calyx of the calyx-only terminal. **D.** Utricle
716 periphery from a vestibular schwannoma patient. Around different HCI, the calyceal CASPR1 label is found in
717 both normal continuous distribution (arrowhead) and in faint and broken distribution (long arrows). **E.** Striola
718 region of the same utricle in **D**. Although some calyceal junctions display a roughly normal continuous
719 distribution of the CASPR1 label (arrowheads), most display faint, broken or largely absent label (arrows). **F**.
720 Higher magnification image from the same patient in **D** and **E.** Two calyces formed by calyx-only terminals are
721 highlighted, one with continuous CASPR1 label (arrowhead) and the other with a patched distribution of this
722 label (long arrow). **G.** Epithelium from a different vestibular schwannoma patient displaying normal CASPR1
723 distribution in calyces from dimorphic terminals (arrowhead) and a double calyx of a calretinin+ calyx-only
724 terminal displaying a partial CASPR1 label in one HC (short arrow) and no CASPR1 in the other HC (long arrow).
725 **Scale Bars: A**, **C**, **D**, and **E**, 25 μm; **B**, 50 μm; **F**, and **G**, 5 μm.

FIGURE 1

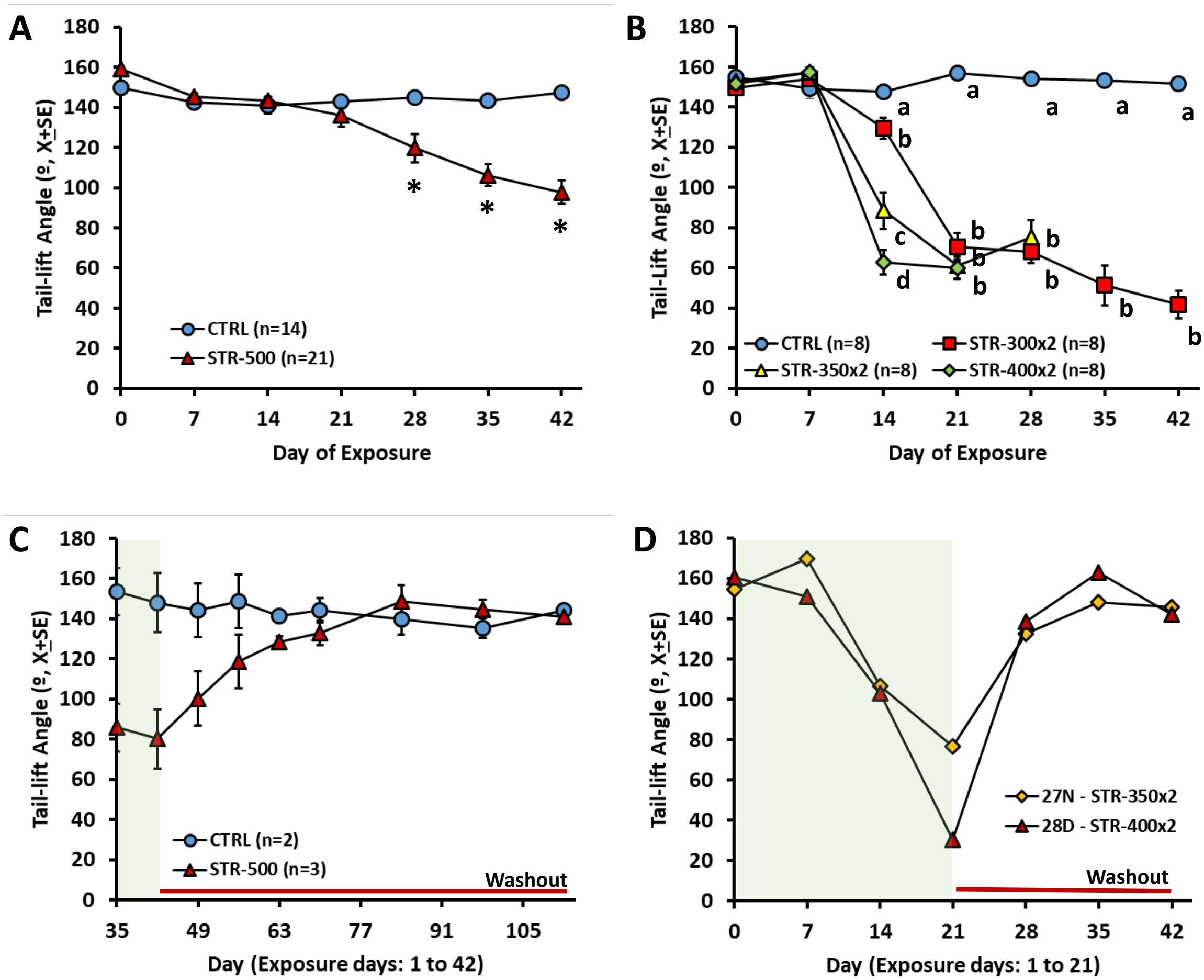

Figure 1. Effects of sub-chronic streptomycin on the tail-lift reflex of rats. Data are mean ± SE minimum angles formed by the nose, the back of the neck and the base of the tail during the reflex behaviour elicited by a tail-lift manoeuvre. Loss of vestibular function causes loss of the anti-gravity trunk extension reflex, which results in ventral curling and thus in smaller angles. **A.** Effects of one injection per day at 0 (CTRL, vehicle control) or 500 mg/kg (STR-500) of streptomycin for 6 weeks, starting at 21 days of age. * $p<0.05$, different from control group after significant day by treatment interaction effect in repeated-measures MANOVA. **B.** Effects of two injections per day at 0 (CTRL, vehicle control), 300 (STR-300x2), 350 (STR-350x2), or 400 (STR-400x2) mg/kg of streptomycin for 6, 6, 4, or 3 weeks, respectively, starting at 21 days of age. The numbers of animals were reduced to 6 in the CTRL group after day 28, and to 7 in the STR-350x2 and STR-400x2 groups after day 21. **a, b, c, d**: groups with different letters are significantly different ($p<0.05$), Duncan's test after significant ANOVA on that day. **C.** Recovery of the tail-lift reflex after the end of exposure in rats administered once a day with 500 mg/kg (STR-500) of streptomycin for 6 weeks. **D.** Loss and recovery of the tail-lift reflex in two individual rats administered twice a day with 350 (STR-350) or 400 mg/kg (STR-400) of streptomycin for 3 weeks, followed by 3 weeks of washout.

FIGURE 2

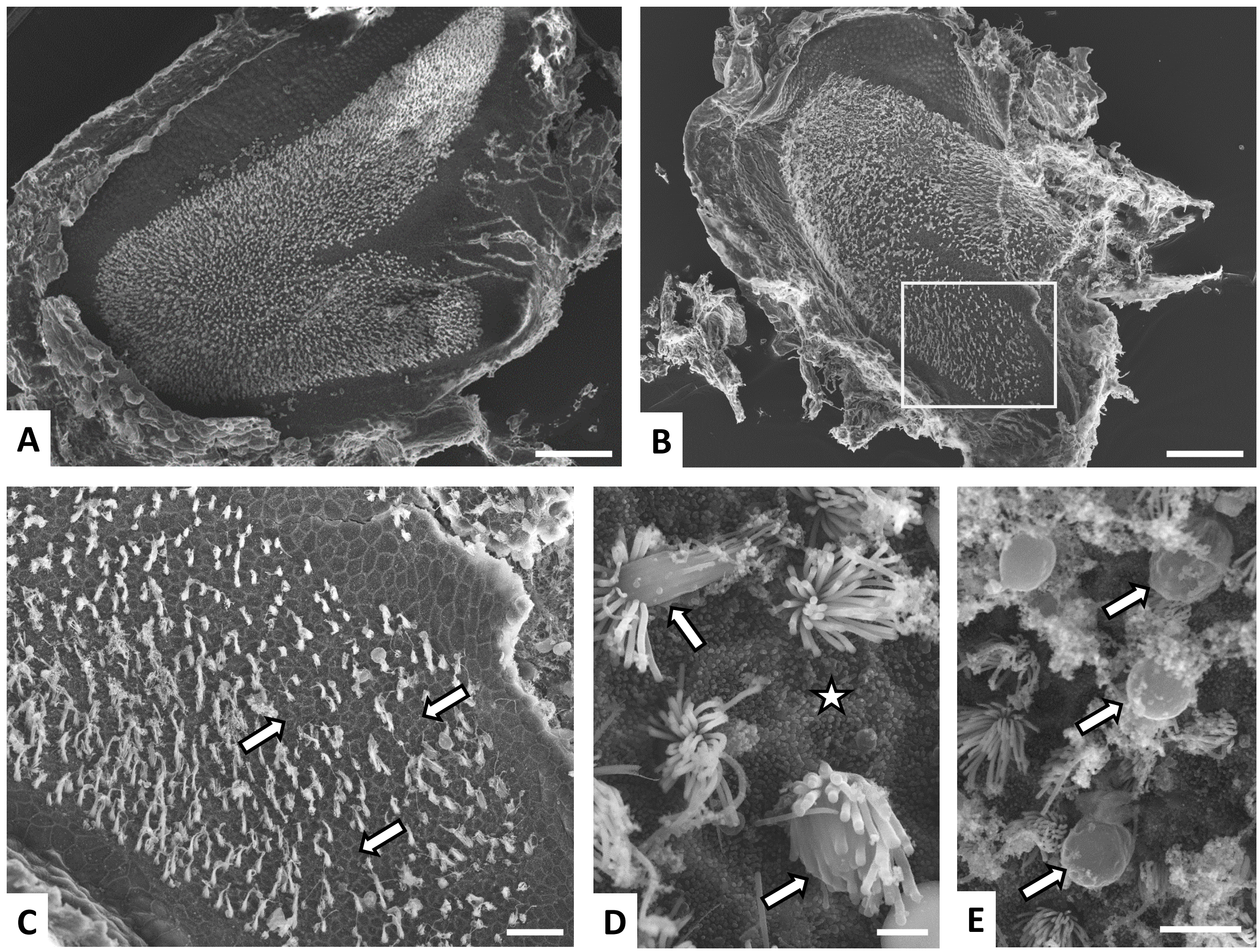

Figure 2. Effects of sub-chronic streptomycin on the vestibular sensory epithelium of the rat as observed in surface preparations of saccules examined by SEM. **A.** Control saccule, showing a high and uniform density of stereocilia bundles throughout the macula. **B.** Effect of one injection per day of 500 mg/kg of streptomycin (STR-500) for 8 weeks. A reduced density of stereocilia bundles is noticeable at this low magnification. The boxed area is shown at higher magnification in panel C. **C.** Higher magnification of the saccule shown in panel B. Note the areas where the lack of stereocilia bundles is evident (arrows). **D and E.** High magnification views of a saccule from a STR-500 rat at 6 weeks of treatment. Note the contacts between the apical edges of supporting cells, marked by a high density of microvellosities, denoting the lack of stereociliary bundles (star), and the bundles showing stereocilia fusion and HC protrusion into the luminal cavity (arrows). **Scale Bars: A** and **B,** 100 μm; **C,** 20 μm; **D,** 2 μm; **E,** 5 μm.

FIGURE 3

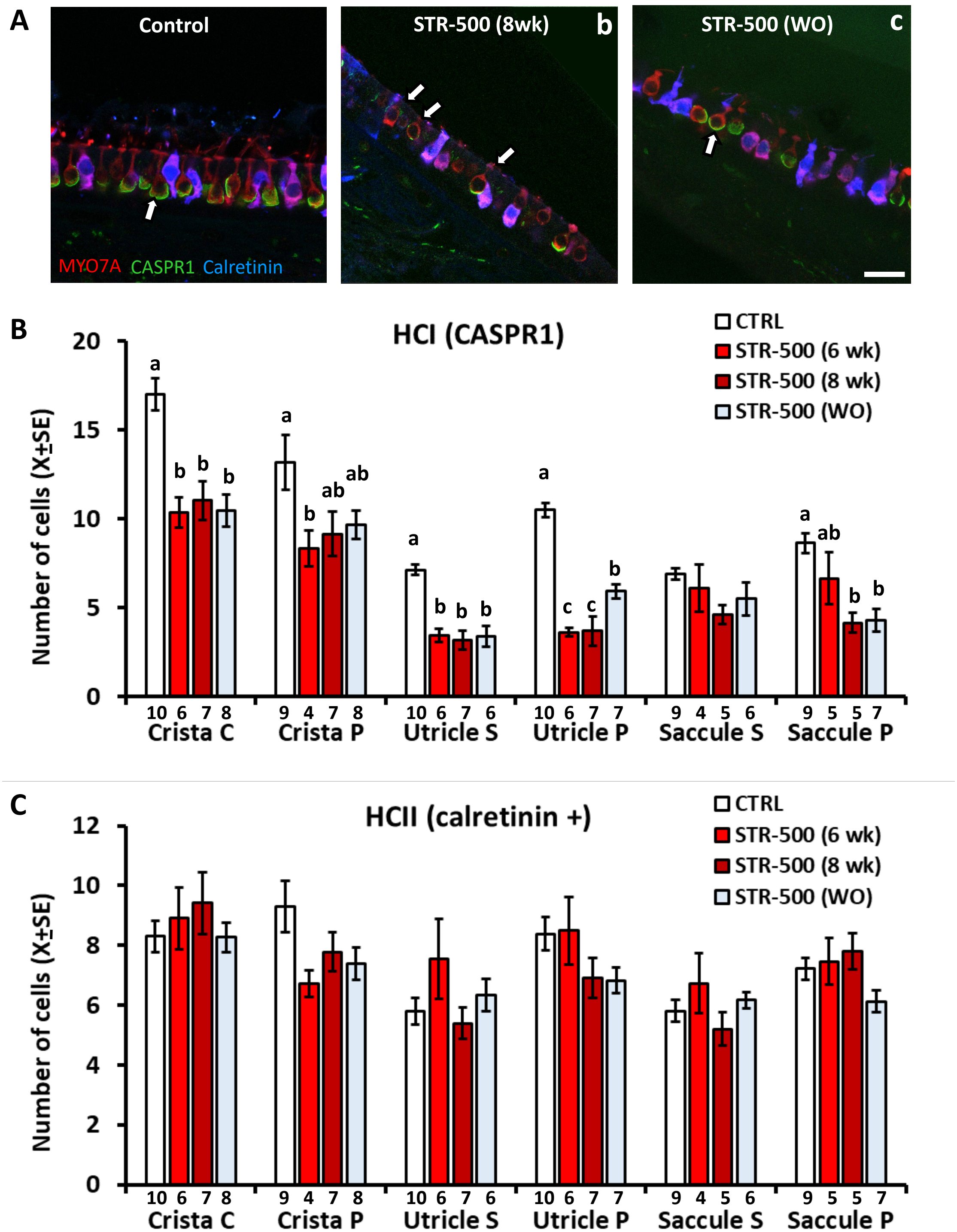
A
Control
STR-500 (8wk)
b
STR-500 (WO)
c
MYO7A CASPR1 Calretinin
B
HCI (CASPR1)
CTRL
STR-500 (6 wk)
STR-500 (8 wk)
STR-500 (WO)
Number of cells (X±SE)
Crista C
Crista P
Utricle S
Utricle P
Saccule S
Saccule P
C
HCII (calretinin +)
CTRL
STR-500 (6 wk)
STR-500 (8 wk)
STR-500 (WO)
Number of cells (X±SE)
Crista C
Crista P
Utricle S
Utricle P
Saccule S
Saccule P

Figure 3. Effects of sub-chronic streptomycin on the numbers of HCI and HCII in the central/striola (C/S) and peripheral (P) regions of the vestibular crista, utricle and saccule, as obtained from confocal images of epithelia labelled with anti-MYO7A (red), anti-CASPR1 (green) and anti-calretinin (blue) antibodies. **A**. Representative images from the peripheral utricle of a control rat **(a)**, a rat treated with 500 mg/kg of streptomycin, once a day, for 8 weeks **(b)**, and a rat treated with streptomycin and allowed 8 weeks of recovery after the end of the treatment **(c)**. HCI were defined by MYO7A+ cells with adjacent CASPR1 label (arrows). To estimate HCIIs, we counted cells with double MYO7A+ and calretinin label. Note the fragmentation of the CASPR1 label in the streptomycin rat (arrows in **b**). To improve readability of the micrograph, a section in the upper right corner of image **b** has been replaced by a drawn triangle. **Scale bar** in (**c**): 20 μm. **B and C.** Counts of HCI **(B)** and HCII **(C)** cells. Data are mean number of cells +/- SE per section. For each animal and epithelial zone, numbers were obtained by averaging counts from 8 areas. Numbers below the bars indicate number of animals included per group. **a, b, c, ab, ac**: groups not sharing a letter are different ($p<0.05$), Duncan's multiple-comparisons test after significant ($p<0.05$) one-way ANOVA. Absence of letters denote group comparisons that resulted in non-significant differences in the ANOVA analysis.

FIGURE 4

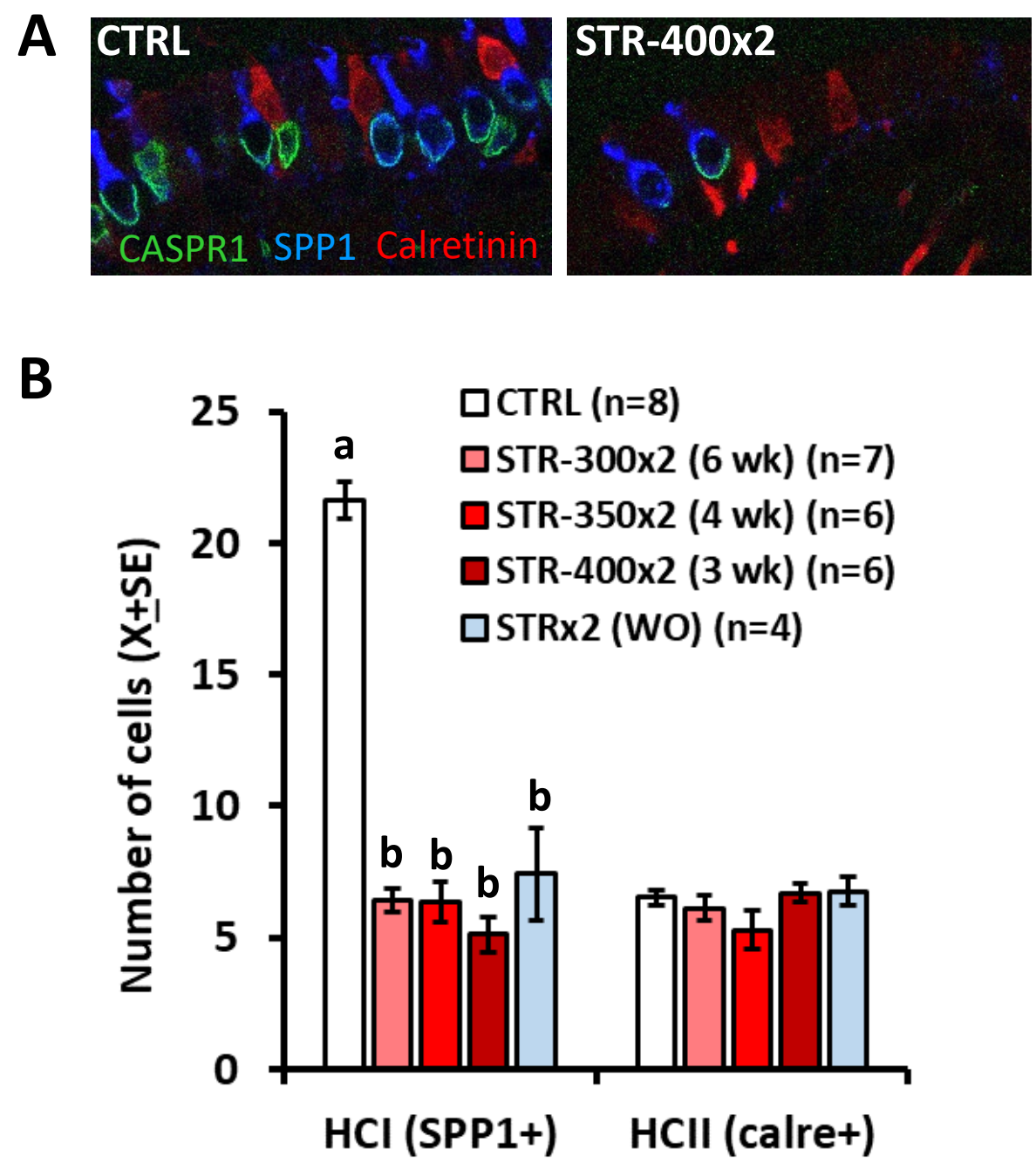

Figure 4. Effects of sub-chronic streptomycin on HC density in the vestibular crista. Samples were from animals receiving 0 (Control, CTRL), 300 (STR-300x2), 350 (STR-350x2) or 400 (STR-400x2) mg/kg of streptomycin, twice a day, for 6, 4, or 3 weeks. The washout (WO) group includes animals allowed 3 weeks of recovery after receiving STR-350x2 or STR-400x2 for 3 weeks. The cristae were labelled with anti-SPP1 (blue), anti-CASPR1 (green) and anti-calretinin (red) antibodies. HCI were defined as SPP1+ cells and HCII were cells with calretinin label. **A.** Partial view of representative sections of control and streptomycin cristae. **B.** Relative numbers of HCI and HCII in the crista sections. Data are mean number of cells +/- SE per transversal section, including central and peripheral regions. **a, b**: groups not sharing a letter are different ($p<0.05$), Duncan's multiple-comparisons test after significant ($p<0.05$) one-way ANOVA. Comparison of HCII group means was non-significant.

FIGURE 5

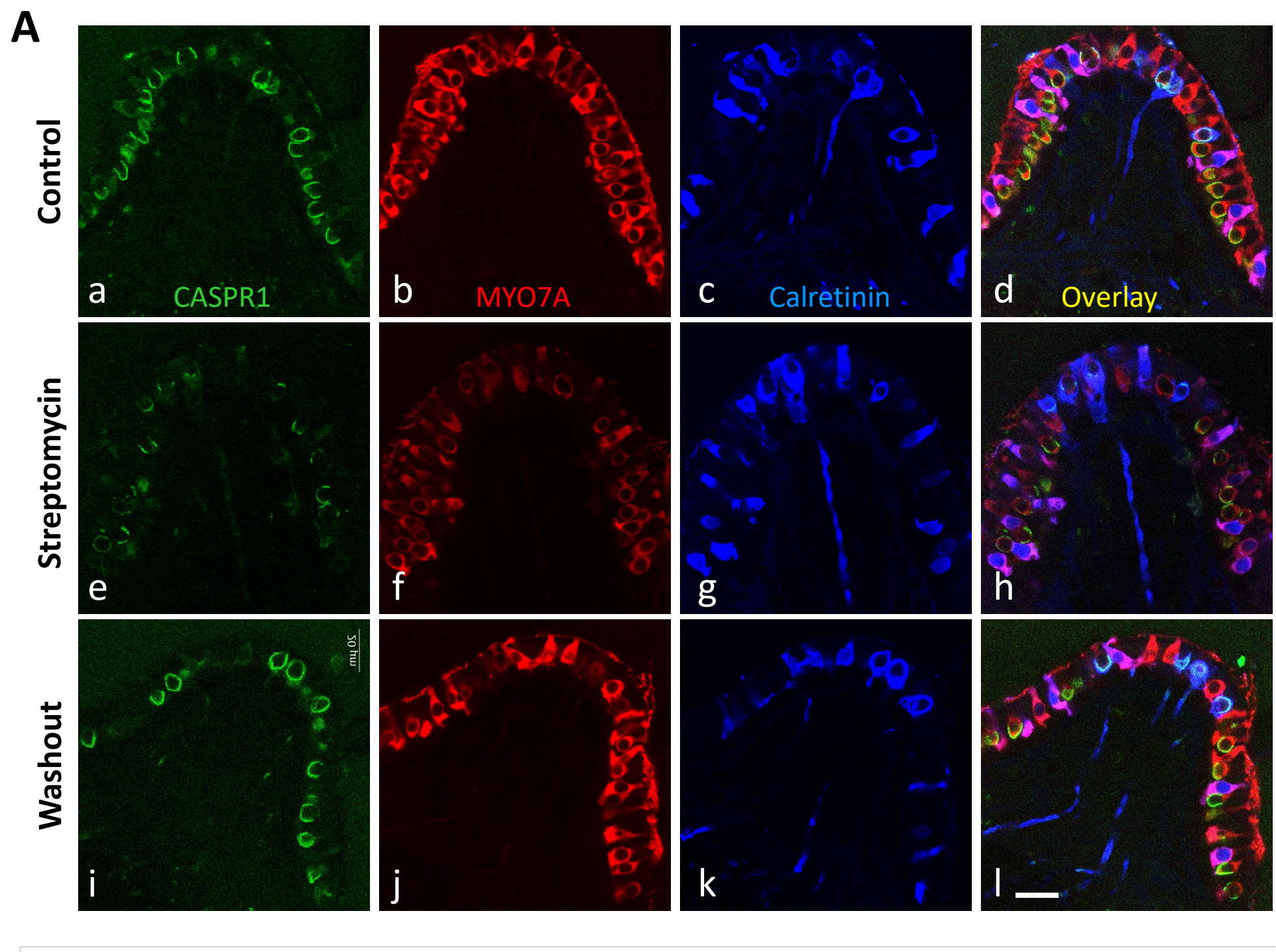

Figure 5. Effects of sub-chronic streptomycin on the expression of CASPR1 in the central/striola (C/S) and peripheral (P) regions of the vestibular crista, utricle and saccule of the rat. The samples were labelled with anti-MYO7A (red), anti-CASPR1 (green) and anti-calretinin (blue) antibodies. **A.** Representative images from mid-crista sections from a CTRL rat (**a** to **d**), a rat treated with 500 mg/kg of streptomycin, once a day, for 6 weeks (**e** to **h**), and a rat allowed recovery during a washout period of 10 weeks after the streptomycin treatment (**i** to **l**). Note the loss and fragmentation of the CASPR1 label caused by streptomycin and its recovery after washout. The intensity of MYO7A label also decreased and recovered. **B.** Quantitative analysis of the CASPR1 fluorescence. Data are normalised arbitrary fluorescence amount per cell +/- SE. For each animal, epithelium and zone, the average amount of fluorescence was obtained from all HCs available for analysis up to 40 cells. Numbers below the bars indicate number of animals included per group. **a, b**: groups not sharing a letter are different ($p<0.05$), Duncan's multiple-comparisons test after significant ($p<0.05$) one-way ANOVA.

FIGURE 6

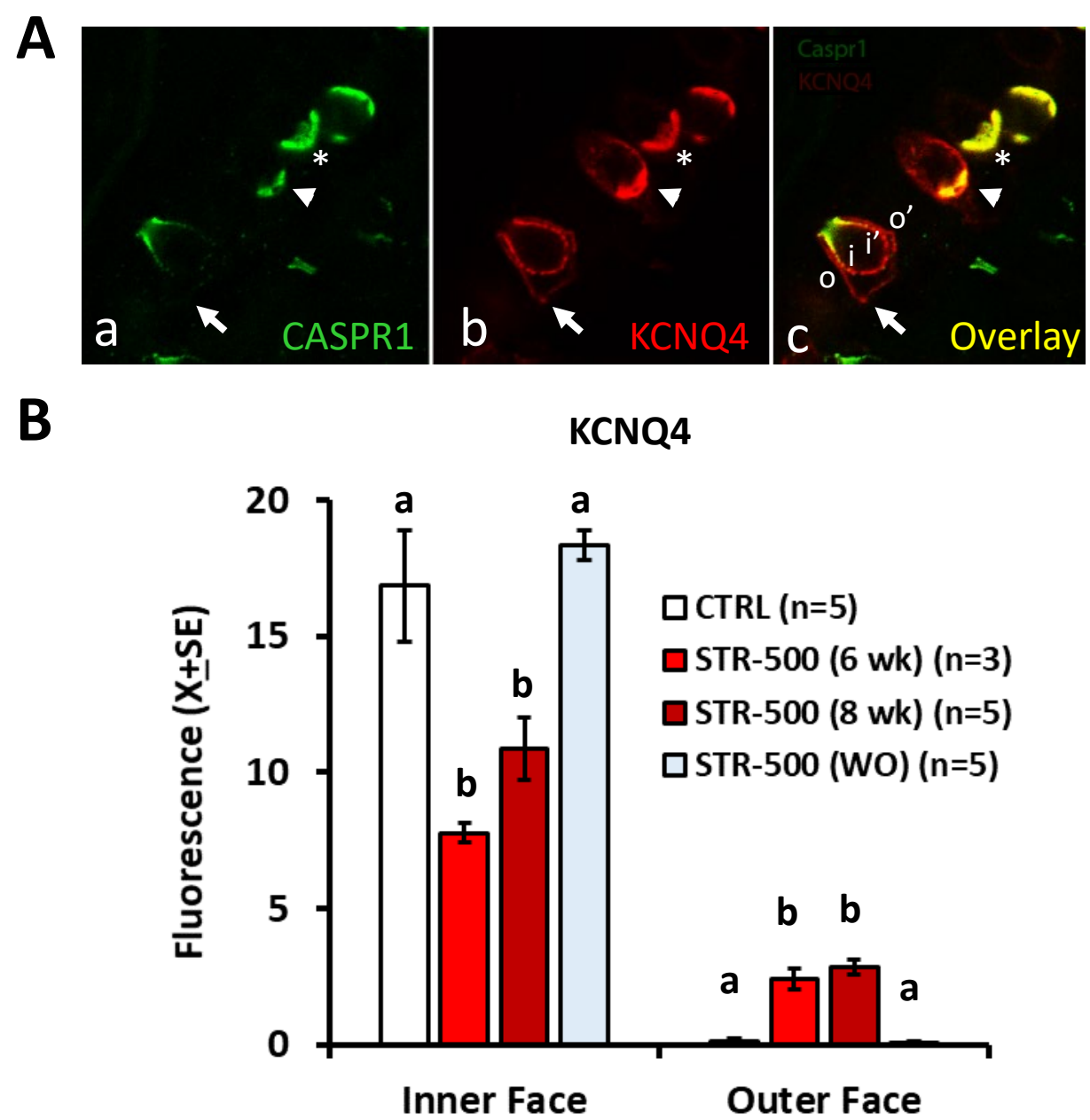

Figure 6. Effects of sub-chronic streptomycin on the distribution of KCNQ4 in the inner and outer membrane of the calyx terminals afferent to HCI in the rat. Vestibular crista were labelled with anti-CASPR1 (green) and anti-KCNQ4 (red) antibodies. **A.** Image from a crista showing the redistribution of KCNQ4. The asterisk indicates a calyx with a control-like co-localisation of CASPR1 and KCNQ4. The arrowhead points to a calyx with CASPR1 loss and reduced co-localisation, with the KCNQ4 antibody labelling a greater area than the CASPR1 antibody. The arrow points to the outer membrane of a calyx with greatly reduced CASPR1 label and redistribution of KCNQ4 throughout both the inner (i and i') and outer (o and o') membranes. **B.** Quantitative analysis of the distribution of KCNQ4 label in the inner and outer face of the calyces in crista from control rats (CTRL), rats treated with 500 mg/kg of streptomycin (STR-500), once a day, for 6 weeks, and rats allowed recovery during a washout period of 8-10 weeks after the streptomycin treatment. Data are mean arbitrary fluorescence units +/- SE. The number of replicas indicate the number of animals included in the analysis per group. **a, b**: groups not sharing a letter are different ($p<0.05$), Duncan's multiple-comparisons test after significant ($p<0.05$) one-way ANOVA.

FIGURE 7

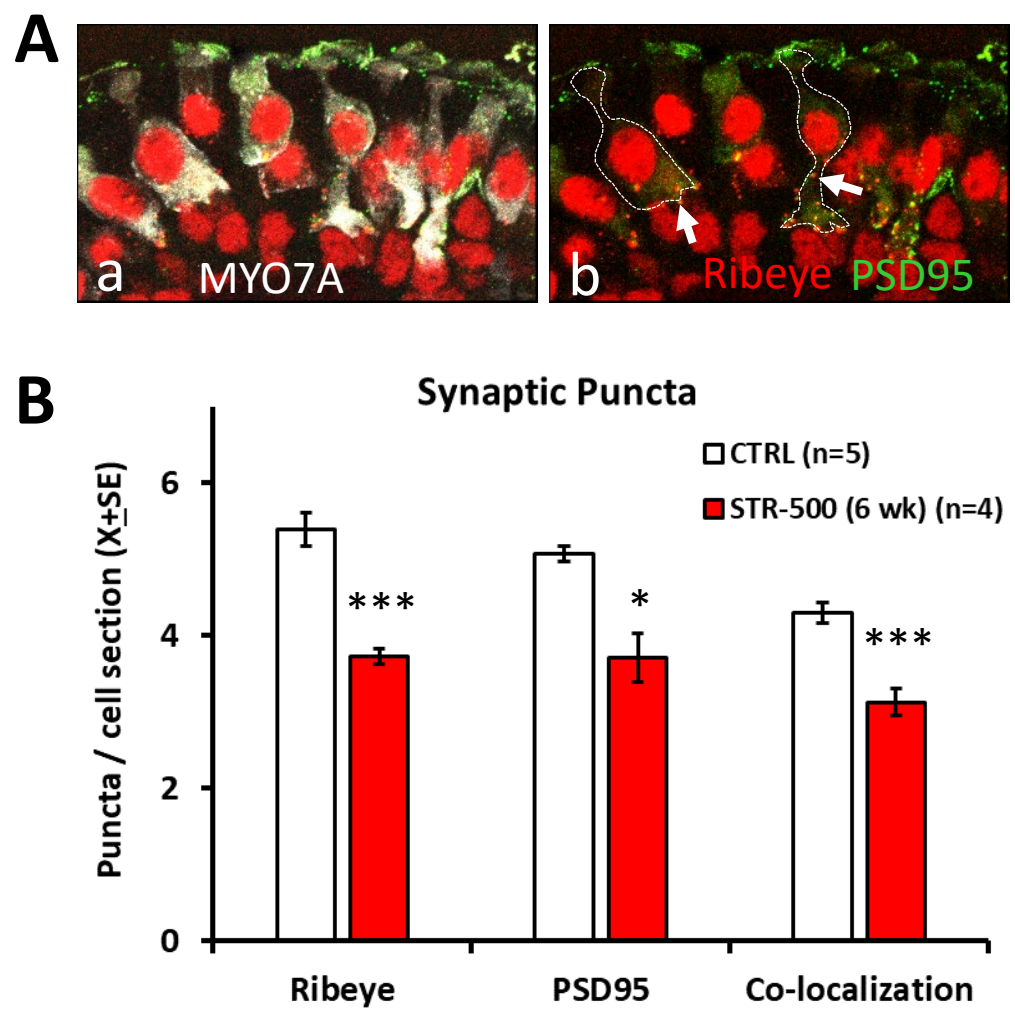

Figure 7. Effects of sub-chronic streptomycin on the numbers of synaptic puncta per 2.6 µm-tick optical sections of HCs in vestibular crista labeled with anti-MYO7A, anti-ribeye and anti-PSD95 antibodies. **A.** Synaptic puncta labelling. In subpanel **a**, the MYO7A label is included to show HC bodies in a control crista. Subpanel b shows the same image without the MYO7A label but including lines delineating the limits of two HCs and arrows pointing to examples of pairs of pre-synaptic (ribeye, red) and post-synaptic (PSD-95, green) puncta. **B.** Mean number of pre-synaptic and post-synaptic puncta, as well as pre- and post-synaptic pairs, +/- SE, from control rats (CTRL) and rats treated with 500 mg/kg of streptomycin (STR-500), once a day, for 6 weeks. The number of replicas indicate the number of animals included in the analysis per group. *: $p< 0.05$, and ***: $p<0.001$, CTRL versus STR-500, Student's T-test.

FIGURE 8

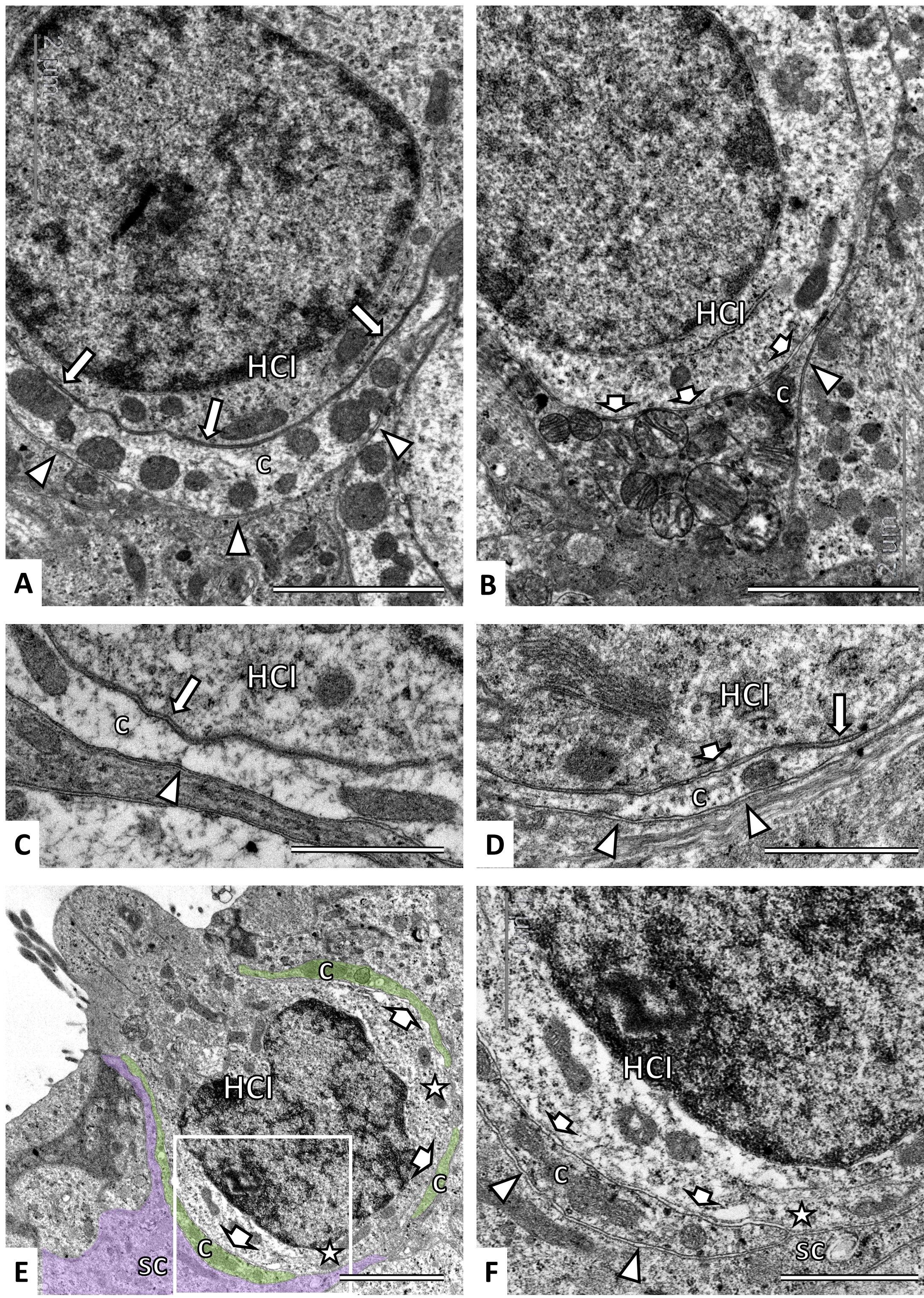

Figure 8. Effects of sub-chronic streptomycin on the calyceal junction and calyx integrity as observed by TEM. **A.** Control crista. The calyceal junction is revealed by the high electron density of the apposing membranes (long arrows) of HCI and inner side of the calyx (c), higher than that found in the outer side of the calyx (arrowheads). **B.** Crista of a rat exposed to 500 mg/kg of streptomycin, once a day, for 6 weeks. In most of the area where the calyceal junction should be found, the apposing membranes show a low electron density (short arrows), similar to that in the outer face of the calyx (arrowhead). **C.** Higher magnification of the calyceal junction (long arrow) and the outer side of the calyx (arrowhead) in a control saccule. **D.** Higher magnification from a crista of a rat exposed to 500 mg/kg of streptomycin, once a day, for 6 weeks. Note the short segment of calyceal junction (long arrow) that remains together with areas devoid of it (short arrow) and the similarity between the latter and the membranes in the outer side of the calyx (arrowheads). **E.** Calyceal junction dismantlement and calyx fragmentation in a HCI showing evidence of ongoing extrusion, from a utricle of a rat exposed to 300 mg/kg of streptomycin, twice a day, for 6 weeks. Note the absence of calyceal junction (short arrows), the fragmentation of the calyx (c, green shadow), and the direct contact between supporting cells and the HCI (stars). The purple shadow highlights one supporting cell (sc). **F.** Higher magnification of the boxed area in panel **E**. Note the similarity of the membranes between the place where the calyceal junction is missing (short arrows) and the outer side of the calyx (arrowheads). Note also the direct contact between a supporting cell (sc) and the HCI (star). **Scale Bars: A**, **B**, and **E**, 2 μm; **C**, **D**, and **F**, 1 μm.

FIGURE 9

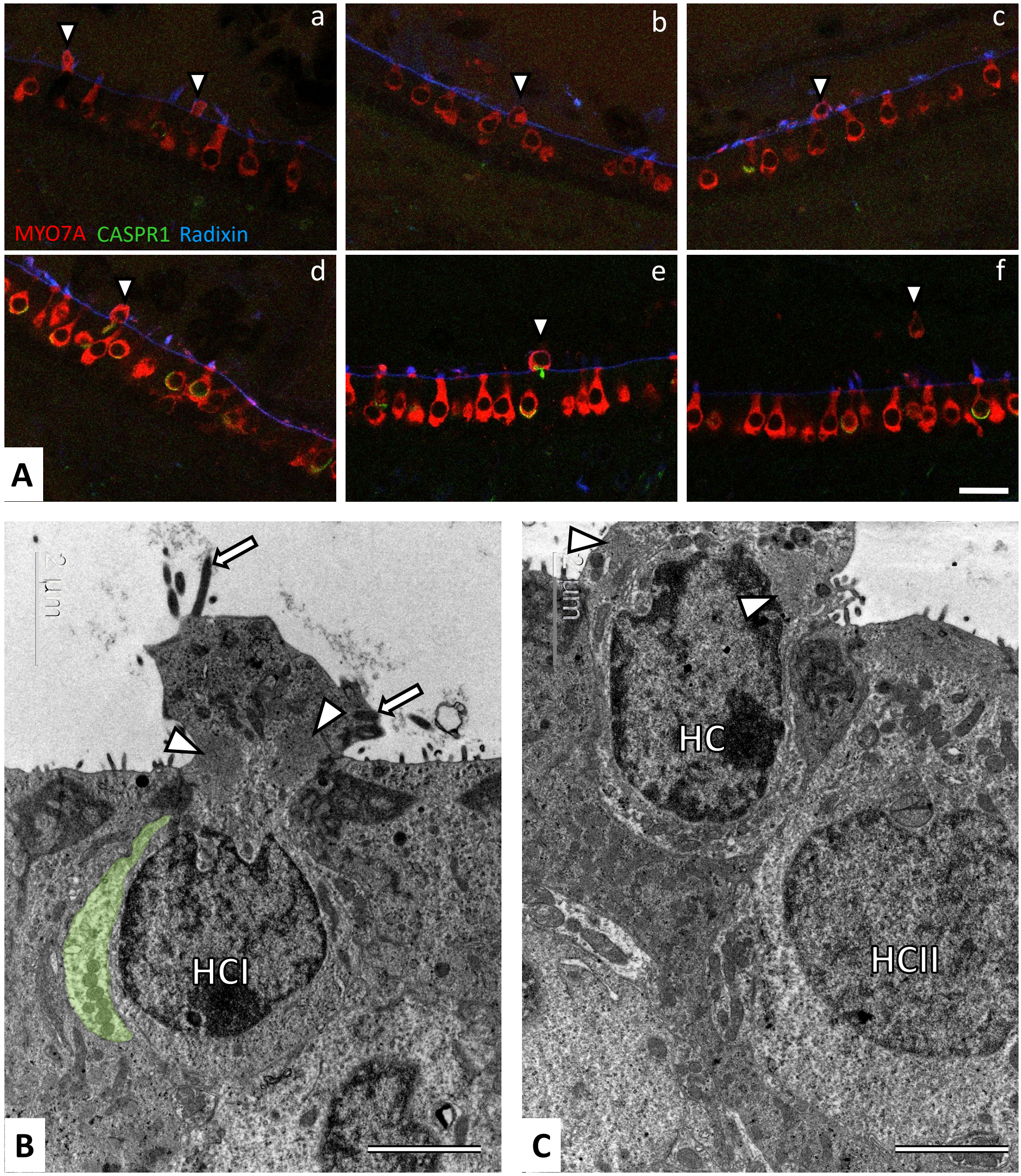

Figure 9. Evidence of HC extrusion in utricles of rats exposed to sub-chronic streptomycin as observed by immunofluorescence and TEM. The images are from rats administered twice a day with 350 mg/kg of streptomycin for 4 weeks, or with 300 mg/kg for 6 weeks. **A.** Utricles immunolabeled with antibodies against MYO7A (red), CASPR1 (green) and radixin (blue). The radixin label of stereocilia and microvilli outlines the surface of the epithelium. Arrowheads point to HCs protruding (**a**, **b**), extruding (**c**, **d**, **e**) or completely extruded (**f**) into the luminal cavity of the utricle. **B** and **C.** TEM images of HCs in a protrusion stage corresponding to that shown in panels **a** and **b**, respectively, of part **A**. Stereocilia (arrows) and striated organelles (arrowheads) identify the extruding cells as HCs. In **B**, note the position of the nucleus of the HC inside the epithelium, and the remnant of a calyx terminal (green shadow) that identifies the HC as a HCI. In **C**, note the position of the nucleus of the HC (unidentified type), half way into the luminal cavity of the utricle. **Scale Bars: A**, 20 µm; **B**, and **C**, 2 µm.

FIGURE 10

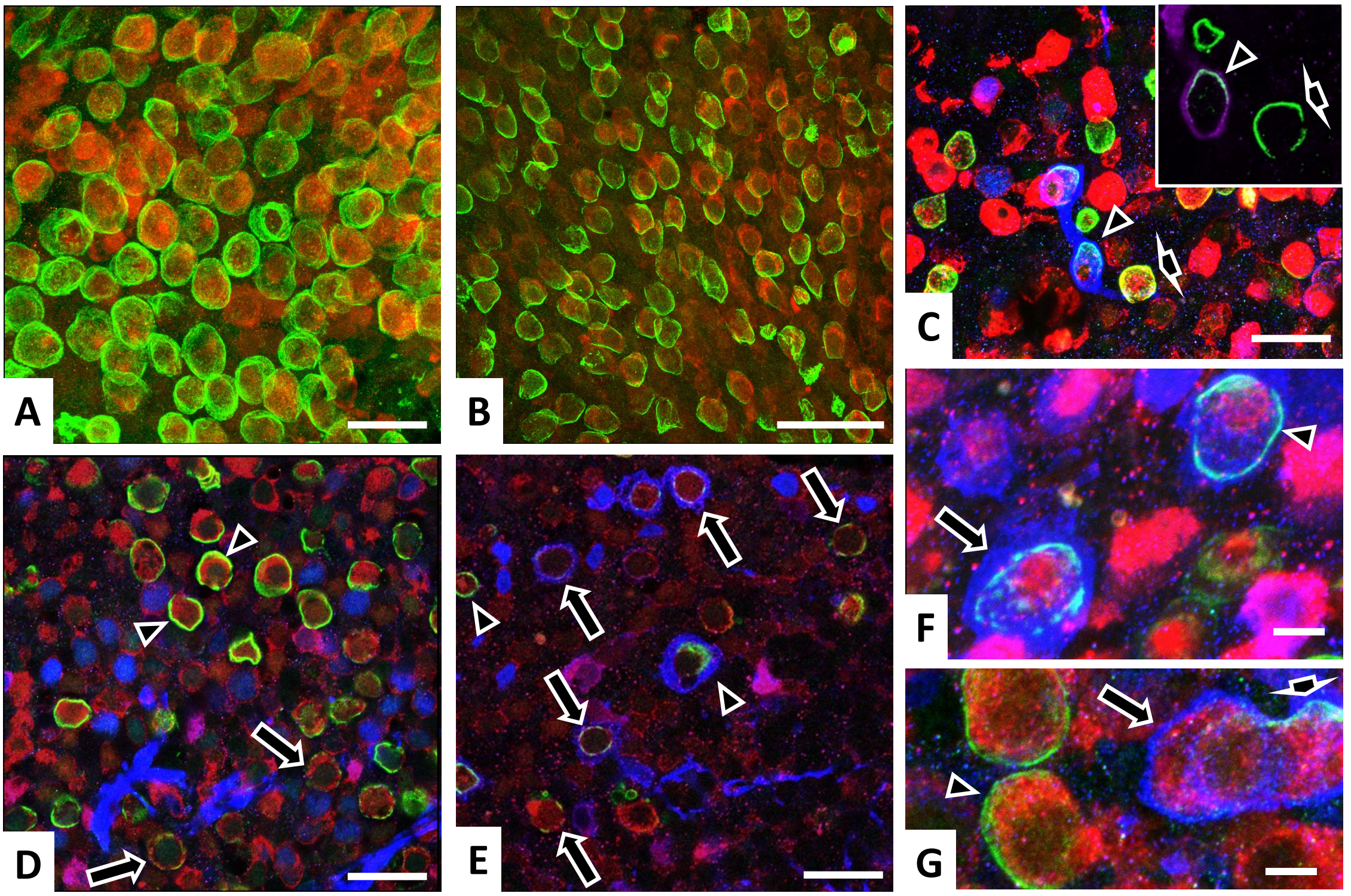

Figure 10. Evaluation of the calyceal junction in vestibular epithelia from patients of vestibular diseases, as revealed by CASPR1 immunolabel (green, light blue when co-localizing with calretinin blue label). In the main panels, HC bodies are labelled with an anti-MYO7A antibody (red). Calretinin is shown in blue in main panels **C** to **F**, and in purple in the inset in **C**. **A**. Epithelium from a patient of Ménière's Disease showing no pathological features. Note the elevated density of HCs and the continuous distribution of the CASPR1 label throughout the calyceal junction area of each HCI. **B.** Epithelium from a meningioma patient, showing also no overt pathology. **C.** Epithelium from a meningioma patient. Note the low density of HCs and the normally continuous CASPR1 label in calyces of both calretinin+ calyx-only terminals (arrowhead) and calretinin- dimorphic terminals (short arrow). The **inset** displays the same two calyces; a thinner stack is shown to highlight the uninterrupted CASPR1 label and its placement in the inner membrane of the calretinin+ calyx of the calyx-only terminal. **D.** Utricle periphery from a vestibular schwannoma patient. Around different HCI, the calyceal CASPR1 label is found in both normal continuous distribution (arrowhead) and in faint and broken distribution (long arrows). **E.** Striola region of the same utricle in **D**. Although some calyceal junctions display a roughly normal continuous distribution of the CASPR1 label (arrowheads), most display faint, broken or largely absent label (arrows). **F**. Higher magnification image from the same patient in **D** and **E.** Two calyces formed by calyx-only terminals are highlighted, one with continuous CASPR1 label (arrowhead) and the other with a patched distribution of this label (long arrow). **G.** Epithelium from a different vestibular schwannoma patient displaying normal CASPR1 distribution in calyces from dimorphic terminals (arrowhead) and a double calyx of a calretinin+ calyx-only terminal displaying a partial CASPR1 label in one HC (short arrow) and no CASPR1 in the other HC (long arrow). **Scale Bars: A**, **C**, **D**, and **E**, 25 μm; **B**, 50 μm; **F**, and **G**, 5 μm.